This paper was written more than thirty years ago, when Professor Libe Washburn was a Postdoctoral Scholar at SIO, and was reluctant to jeopardize his career in Oceanography by joining in a publication expressing the highly controversial views of his PhD advisor (CHG) about turbulence and fossil turbulence. Since Washburn is now a distinguished, and tenured, Professor at UCSB, he has consented to the present publication. Vastly different turbulence parameters result when the extreme intermittency in space and time of oceanic turbulence is not taken into account. Most oceanographers claimed, and still claim, the difference is due to vibrations of towed sensors. Not true.

"Mixing Events in the Seasonal thermocline During MILE: Intercomparison of Turbulence Sampling Techniques"

Libe Washburn[*] *and Carl H. Gibson*[**]

[*]Department of Applied Mechanics and Engineering Sciences, University of Calif., San Diego

[**]Department of Applied Mechanics and Engineering Sciences, and Scripps Institution of Oceanography University of Calif., San Diego

ABSTRACT

Observations of mixing processes within the seasonal thermocline conducted from a towed instrument platform during the 1977 Mixed Layer Experiment (MILE) are compared to dropsonde measurements. Mixing activity was found to be concentrated in small patches occupying about 4% of the total record. Dissipation rates of velocity, temperature and salinity, ϵ, χ_T, and χ_S were estimated for individual patches from microconductivity spectra. Values of ϵ and χ_T overlapped the ranges of dropsonde values reported by Dillon and Caldwell (1980) for patches at the same depths, 30-40 m. Mean values for the 5.7 km tow body record were $\bar{\epsilon} = 2 \times 10^{-5} \mathrm{cm}^2/\mathrm{s}^3$ and $\bar{\chi}_T = 1.0 \times 10^{-6}\,°C^2/s$. From the spectral peak wavenumber, values of ϵ in most of the microstructure patches were less than the minimum $\epsilon_{min} = 25\nu N^2$ necessary for turbulence to exist, even though Cox numbers $\overline{(\nabla T)^2}/(\nabla \bar{T})^2$ in the patches were as large as 4009 suggesting strong turbulence at a previous time. Previous dissipation rates ϵ_o at the time of turbulence fossilization were estimated to be as large as 2.8 cm^2/s^3, with an average $\bar{\epsilon}_o = 1.1 \times 10^{-2} \mathrm{cm}^2/s^3$. Estimated values of temperature dissipation rates χ_{To} at fossilization were as large as $8.3 \times 10^{-3}\,°C^2/s$ with average $\bar{\chi}_{To} = 3.2 \times 10^{-5}\,°C^2/s$. From Washburn and Gibson (1982b) χ_T is approximately lognormal, with variance $\sigma^2_{\log\chi} = 1.0$ decade and with mode $\chi_T = 4 \times 10^{-10}\,°C^2/s$ which is 2.5×10^3 times less than the mean. Background values of χ_T at seasonal thermocline depths reported by Lange (1981) from a vertically profiling dropsonde were in the range 10^{-9} to $6 \times 10^{-8}\ °\mathrm{C}^2/\mathrm{s}$, factors of $10^2 - 10^3$ less than the mean and comparable to the mode of χ_T in this region. Apparently, the Lange (1981) values underestimate the space average due to undersampling. The present intercomparison suggests such large underestimates of the actual ϵ, χ and C average values may be a characteristic result for isolated dropsonde profiles in layers with intermittent turbulence where mode values tend to be much less than mean values. High wavenumber portions of some microconductivity spectra were dominated by salinity and indicate that salinity variance dissipation rates χ_S in the microstructure patches were as large as $3 \times 10^{-7}(\,°/_{oo})^2/s$. Because $\chi_T(\partial \bar{S}/\partial z)^2/\chi_S(\partial \bar{T}/\partial z)^2$ was found to be

of order 1.0, the vertical diffusivities of temperature K_T and salinity K_S are apparently of comparable magnitude. Two independent methods gave equal estimates of ϵ_o for the microstructure patches. ϵ/ϵ_o ratios ranged from 0.7 to as small as 6×10^{-7}. Since ϵ/ϵ_o ratios were less than 1.0 in all patches the microstructure is interpreted as fossil turbulence at least at the largest scales. In several patches where ϵ was less than $25\nu N^2$ the turbulence should be fossil at nearly all scales in most of the volume of the patch. However, within these strongly damped patches the temperature gradient spectra were broadened, indicating a wide range of $\epsilon/\nu N^2$ values including some exceeding the critical value of 25 and thus some residual localized turbulence in all patches. Because much of the observed microstructure is fossil, the turbulent mixing processes have been undersampled by both the towed body and the dropsonde measurements. The towed body data gives better convergence to the space average than the dropsonde data because of greater sample size, but neither data set was large enough to include the dominant mixing in a state of completely active turbulence with $\epsilon \approx \epsilon_o$.

1. INTRODUCTION

The Mixed Layer Experiment (MILE) was a joint Canadian-United States study of mixed layer processes which was carried out at Ocean Station P (145°W, 50°N) from 19 August to 7 September 1977. Three ships, the Canadian weather ship *Quadra*, the NOAA ship *Oceanographer*, and the USNS *de Steiguer*, operated in a 30×30km region around a three mooring triangle. Davis *et al.* (1981a,b) describe the evolution of the heat and momentum fields based on data from the moorings. An important goal of the MILE experiment was to study the turbulent mixing processes by which the storms of early autumn erode the open ocean summer thermocline. In an effort to understand the details of these mixing processes, direct, small scale microstructure measurements of temperature and velocity were conducted from a number of instrument platforms during MILE.

A corrolary goal of MILE was to intercompare towed body and dropsonde turbulence measurement techniques. The present paper and Washburn and Gibson (1982a,b) discuss horizontally towed microstructure measurements made from the *Oceanographer* in the layer of maximum vertical density gradient at the pycnoline, in the depth interval 30-40m. In the present paper, these horizontal measurements are compared to vertically profiling dropsonde measurements of Lange (1981) from the *de Steiguer* and dropsonde measurements of Dillon and Caldwell (1980), Dillon (1982a) and Caldwell *et al.* (1980) made from the *Oceanographer* at times alternating with the times of towed profiles.

As discussed by Gibson (1981a), sampling turbulence in the ocean is no easy matter and rather spectacular discrepancies have arisen between estimates of turbulence parameters in the same layer of the ocean depending both on how the turbulence is sampled and on how the same microstructure data is interpreted. For example, a discrepancy of 3-4 orders of magnitude has existed for several years between measured values of the velocity and temperature dissipation rates ϵ and χ in the "core" (maximum velocity) layers of both Atlantic and Pacific equatorial undercurrents depending on whether the instruments were towed or dropped. Williams and Gibson (1974) and Belyaev *et al.* (1975) find ϵ values of $10^{-1} cm^2/s^3$ and χ values of

10^{-5}–10^{-4} °C^2/s at core depths with towed bodies, compared to ϵ values of $(2–4) \times 10^{-5}$ cm^2/s^3 by Crawford (1976) and Crawford and Osborn (1980) and χ values of $(2–10) \times 10^{-8}$ °C^2/s by Gregg (1976) and $(1.1–3{,}400) \times 10^{-9}$ °C^2/s by Osborn and Bilodeau (1980) using various dropsondes. The discrepancy is attributed to 'vibrations' in towed body measurements by Gregg (1976) and Crawford and Osborn (1980). However, Gibson (1981a) attributes the discrepancy to large undersampling errors in dropsonde measurements due to the large intermittency of the turbulence at the strongly stratified core depths.

The results of the present intercomparison of towed body and dropsonde dissipation measurements from the seasonal thermocline may be relevant to the equatorial undercurrent core layer because both are regions of maximum vertical density gradient. Although the distributions of mean vertical shear for the two layers are different, the effects of the maximum stratification on the turbulence should be the same; that is, both the mixing rate and the intermittency may be maximized compared to layers above and below. Dropsonde profiles of Lange (1981) and Dillon and Caldwell (1980) show minimum ϵ and χ values at seasonal thermocline depths, just as Osborn (1980) and Gregg (1976) show minimum values of ϵ and χ, respectively, at equatorial undercurrent core depths. However, as proposed by Gibson (1981a) and as indicated by the present towed body measurements, turbulence and mixing (and ϵ and χ) may actually be at *maximum* levels for both the seasonal thermocline and the equatorial undercurrent core layer, not minimum levels. The minima in ϵ and χ observed by the various dropsondes may be only a manifestation of undersampling caused by maximum intermittency of the turbulence process in these strongly stratified layers.

Turbulence intercomparison measurements at sea are difficult because of large variability in time and space of the background conditions. However, during MILE the solar heating and the cooling by wind mixing were roughly in equilibrium. Davis *et al.* (1981a) found that the 12.5 hour-average depth of the 9°C and 10°C isotherms varied by 5 m or more during MILE compared to a deepening trend during this period of less than a meter. CTD profiles by S. P. Hayes (personal communication, 1978) also show little qualitative change over the MILE

period compared to the day to day variability. Therefore, the microstructure comparisons in the present paper will be made assuming that the only relevant external parameter is the wind speed at the time of observation and that the previous history or the date of the observation are less important.

Washburn and Gibson (1982b) show that turbulence and mixing activity in the seasonal thermocline is concentrated in a small fraction of the fluid volume. In this paper we report detailed analysis of the microstructure in 33 active patches and examine the contribution of these patches to various averages within the layer. Comparisons are made with the dropsonde measurements of Lange (1981) and Dillon and Caldwell (1980). The VMSR (velocity microstructure recorder) used by Lange (1981) is the most sensitive to temperature fluctuations of the three microstructure systems deployed in MILE but collected the least data: Only 12 profiles were successful giving about 120 meters of record within the depth zone of the seasonal thermocline. χ values reported by Lange (1981) within this region were in the range $(1-6) \times 10^{-9}$ $°C^2/s$ for days with light winds (September 2-3, wind speed 4-6 m/s) and about $2.5 \times 10^{-9} - 6.0 \times 10^{-8}$ $°C^2/s$ for moderate winds (September 4, 7.7 m/s). Dillon and Caldwell (1980) used a rapidly deployable dropsonde and collected 381 successful profiles. They report (isotropic) C values of 3-60 for the depth range 30-40 m during light winds (September 1, 5.5 m/s) 8 hours after a storm, giving much larger χ values in the range $(0.1-7) \times 10^{-6}$ $°C^2/s$ (assuming $\partial \bar{T}/\partial z = 0.28$ °C/m from their vertical temperature profiles). During one of the stronger storms of the MILE experiment a few hours later (September 1, 15.5 m/s) they found C values were 3-9,000 at 30-40 m giving χ values from 6.6×10^{-8} to 2×10^{-4} $°C^2/s$.

Why are the Dillon and Caldwell (1980) χ values as much as 10^4 times larger than the Lange (1981) values? It seems likely that the larger values reflect the larger sample size generated by the more rapidly deployable dropsonde just as the larger range of χ values observed by Osborn and Bilodeau (1980) in the equatorial undercurrent core probably reflects their larger sample size compared to Gregg (1976) rather than any difference in the flows. What are the space time averages of χ, C, and ϵ in the MILE seasonal thermocline? Dillon and Caldwell (1980) conclude that it is impossible to give a reliable estimate of ϵ from their data because

temperature gradient spectra were often unresolved in this region. Likewise their estimates of C, and consequently of χ, are extremely variable with differences of up to 3 orders of magnitude. Because of this variability and the fact that on a given day their record length within the seasonal thermocline is small, determination of mean values at a given time is very uncertain and is not done by Dillon and Caldwell (1980). Because the total record length from the Lange (1981) data is even smaller than that of Dillon and Caldwell (1980), it is also impossible to estimate mean values of χ from Lange (1981). In this paper we present estimates of mean values of χ, C, and ϵ based on individual patches of microstructure from a total record length of 5700 m obtained during a horizontal tow through the seasonal thermocline. These towed data were obtained on September 7, several days after the storm in which the Dillon and Caldwell (1980) data were collected. Values of ϵ and C in individual patches from these towed profiles span the range of values reported by Dillon and Caldwell (1980) in the seasonal thermocline. The mode of the distribution of χ estimated from these towed data is close to the χ profile values of Lange (1981) in the seasonal thermocline region. This is expected since a few samples of a highly intermittent random variable with a nearly lognormal distribution will tend to sample the most probable value of the distribution, the mode.

The viscous dissipation rate ϵ is also a crucial parameter in understanding the dynamics of small scale mixing processes in the ocean. However, estimating ϵ by direct measurement of velocity gradients on viscous scales is much more difficult than direct χ measurements from small scale temperature gradients. Dillon and Caldwell (1980) report several inferred values of ϵ from the seasonal thermocline which are less than $10^{-6}\text{cm}^2/\text{s}^3$; substantially below the noise level of the most advanced velocity measuring probes such as the airfoil shear probe used by Gargett and Osborn (1981) or the heated thermistors used by Lange (1981) during MILE. The Dillon and Caldwell (1980) ϵ estimates were made by fitting temperature gradient spectra to the diffusive cutoff portion of universal form predicted by the turbulent mixing theory of Batchelor (1959), and in this paper we use the wavenumber at the spectral peak. According to the theory the wavenumber at the spectral peak should be proportional to $(\epsilon/\nu D^2)^{1/4}$ (see (1) in Section 3

of this paper). As long as the spectrum has the universal form, fitting any portion should give the same value of ϵ. The method has also been used by other investigators, including Schedvin (1979) and Caldwell *et al.* (1980). However, as pointed out by Dillon and Caldwell (1980), if the patch contains various ϵ values the spectrum will be broadened and their algorithm will be biased to the largest ϵ values in the patch. Similarly, our method of basing ϵ on the peak wavenumber is biased toward smaller ϵ values, since adding two Batchelor spectra with the same χ values but different ϵ will produce a spectrum with peak determined by the smaller ϵ value. Gibson (1982b) concludes that the Dillon and Caldwell (1980) and Caldwell *et al.* (1980) microstructure is fossil turbulence in various stages of decay, but Gibson (1982a) shows that the same proportionality constant and spectral shape should be found near the spectral peak for either actively turbulent or fossil turbulence microstructure. Oakey (1982) has recently verified the temperature gradient ϵ technique by estimating the proportionality constant and spectral shape with simultaneous velocity and temperature measurements in the ocean. He found good agreement between ϵ from direct velocity measurement and ϵ inferred from the temperature gradient spectrum. Gibson (1982a) shows (ignoring possible variability in ϵ and N) that many of the Oakey (1982) microstructure regions sampled are completely nonturbulent fossils and that all regions are fossil at the largest scales by comparison with the Gibson (1980) theory, so the agreement between direct and indirect ϵ values is consistent with the theoretical prediction that the universal form should be valid for fossil turbulence spectra at the diffusive cutoff.

For the seasonal thermocline the Lange (1981) ϵ values appear inexplicably large compared with the pattern of χ values in the same region. Lange's heated thermistor ϵ profile values were $10^3 - 10^4$ times larger than the minimum ϵ values in the microstructure patches detected by either the Dillon and Caldwell (1980) dropsonde or the present towed body using either the "peak" or "tail" temperature gradient ϵ technique. This is in contrast with the χ

profiles reported by Lange (1981) which were $10^3 - 10^4$ times smaller than minimum χ values from these towed data and $10^1 - 10^2$ times smaller than minimum χ values inferred from Dillon and Caldwell (1980). Since high ϵ values should always be associated with high χ values in regions of large vertical temperature gradient (see Section 3, (9)), the mismatch in profiles of Lange (1981) is surprising.

Values of ϵ obtained from temperature spectra allow inferences about the state of fluid motion within microstructure regions. Two fundamental scales may be evaluated if ϵ and N are known: the Richardson (or Ozmidov) length $L_R = \epsilon^{1/2} N^{-3/2}$ and the Kolmogoroff length $L_K = \nu^{3/4} \epsilon^{-1/4}$, where N is the Brünt-Väisälä frequency and ν is the kinematic viscosity. As discussed by Gibson (1980), L_R and L_K represent limits on the range of scales over which 3-dimensional turbulence can exist. Gibson (1980) proposes that the criterion for the existence of active turbulence in a stratified fluid should be $\epsilon \geqslant 30 \nu N^2$. Gibson (1981b, 1982c) present a wavelength criterion for the existence of turbulence; that is, $1.2\, L_R \geqslant \lambda \geqslant 15\, L_K$. These criteria are in good agreement with measurements of Stillinger (1981) which give $\epsilon \geqslant 25 \nu N^2$ and $1.4\, L_R \geqslant \lambda' \geqslant 15.4\, L_K$, where λ' is an overturning scale approximately equal to the wavelength λ. Buoyancy forces suppress vertical motions on scales larger than L_R while at scales smaller than L_K viscous stresses damp the turbulent motion and leave the fluid in a state of locally uniform straining. Increasing ϵ tends to increase the range of vertical scales lying between L_R and L_K (the inertial subrange of the turbulence) and hence increase the vertical scales over which turbulent transport may occur. Weinstock (1978) argues that most of the transport within a turbulent region in a stratified fluid occurs at scales within the inertial subrange, although a significant amount of kinetic energy may reside in scales larger than L_R. This is equivalent to the criterion of Gibson (1981b, 1982c) that turbulent transport may occur only over a limited range of vertical wavelengths, as discussed above.

In two-thirds of the patches examined, we find that values of ϵ from our towed data in the seasonal thermocline are smaller than 25 νN^2, thus indicating that, based on mean quantities, no turbulence can exist on any scale in these patches. However, as discussed previously, the broad distribution of both ϵ and N will permit some residual turbulence even in such patches. Therefore the small scale temperature and salinity fluctuations in the patches were produced by active turbulence but are almost completely fossil temperature and salinity turbulence at the time of observation. In the other third of the patches ϵ values were larger than $25\,\nu N^2$, but in all cases ϵ values were smaller than $\epsilon_o' = 13\mathrm{DCN}^2$. This indicates that ϵ values within these microstructure patches are not sufficient to overturn on the vertical scales implied by the values of C in these same patches. ϵ_o' is less than or equal to the dissipation rate at fossilization ϵ_o. As proposed by Gibson (1980), $\epsilon_o \approx 13D\,C_o\,N^2$ and the ratio $\epsilon/\epsilon_o' \equiv A_T^2$, where A_T is the turbulence activity parameter. According to the Gibson (1980) theory A_T must be >1 for completely active turbulence. Since $\epsilon/\epsilon_o' < 1$ then $A_T < 1$, so none of the microstructure patches are actively turbulent at the largest wavelengths of the temperature fluctuations; that is, for wavelengths λ where $1.2L_{Ro} \geqslant \lambda \geqslant 1.2\,L_R$. Using the wavelength criterion discussed previously, active turbulence can exist in these patches only for λ values in the range $1.2\,L_R \geqslant \lambda \geqslant 15\,L_K$. For the present data, the largest inferred overturning wavelength at fossilization $1.2\,L_{Ro}$ was 620 cm in a patch where the measured $1.2\,L_R$ was only 0.8 cm. The largest overturning wavelength $1.2\,L_R$ measured was 13 cm in a patch where $1.2\,L_{Ro}$ was 63 cm (see Table 1). Because the microstructure patches are fossil turbulence remnants, the previous dissipation rates must have been much larger than those measured, at least as large as the inferred values of ϵ_o and χ_o. Further discussion of the techniques used to infer hydrodynamic activity from parameters such as A_T and ϵ_o' are given in Section 3.

The largest value of A_T observed in the present data was 0.78, indicating almost completely active turbulence, in one 6.6 m long patch with Cox number of 271 and $\epsilon/\nu N^2 = 219 >> 25 = (\epsilon/\nu N^2)_{\min}$. However, the patch with the largest Cox number of 4009 had an A_T value of only 0.012 and $\epsilon/\nu N^2 = 1.0 << 25$. $C_o = C/A_T$ for the latter patch was

3.3×10^5 compared to only $C_o = 347$ for the patch with $A_T = 0.78$ (from (7), Section 3). Therefore the most actively turbulent patch; that is, the patch with largest A_T value, makes a negligible contribution to either the space average $\bar{\chi}$ or space-time average $<\chi>$ compared to a completely fossil patch with large χ_o. The actual space-time average Cox number $<C>$ is probably bounded by the space average $\bar{C} = 42$ and the space average $\bar{C}_o = 1282$, at least over a previous time period comparable to the age of the patch with the largest C_o value. At present no reliable method exists for estimating the age of a fossil turbulence patch, so it is not clear whether the space-time average should be closer to $\bar{C}$ or $\bar{C}_o$, or what time period is represented by such an estimate of the space-time average. Gibson (1982c) estimates the age of a deep ocean fossil patch detected by Gregg (1980) as several days using the measured Thorpe displacement scales ζ, but ζ values are not available for the present data and the Gibson (1982c) technique is quite approximate and requires several questionable assumptions. Dillon (1982a) estimates time constants $\overline{\delta T^2}/\chi$ which are less than N^{-1} for the Dillon and Caldwell (1980) microstructure patches, and Dillon (1982b) estimates time constants $\overline{g\rho'\zeta}/\epsilon$ which are less than N^{-1}. From these small values Dillon concludes that the patches cannot be fossil turbulence at any scale, contrary to the conclusions of Gibson (1982c). The difference in interpretation appears to be due to differences in calculational techniques, differences in assumptions about the appropriate parameter relationships, and differences in assumptions about the necessary properties of fossil turbulence. All these differences arise from the present poor state of understanding of stratified turbulence. Further discussion of these differences is beyond the scope of the present paper.

2. Experimental Description and Data Analysis

Data of this paper were collected on 7 September 1977 in the depth interval 30-40m in the seasonal thermocline during MILE from the *Oceanographer*. Temperature data were obtained from the signal of a small conductivity probe (2.5 mm electrode length), referred to here as a microconductivity probe, mounted on an instrument platform which was towed at a nearly constant depth. For the temperature-salinity variations of these data the microconductivity signal was usually dominated by fluctuations of temperature at all measured wavenumbers although a few regions were found in which the highest wavenumbers were dominated by salinity. A factor of 1.16 °C/(mmho/cm) is used to convert conductivity to temperature as discussed by Washburn and Gibson (1982a). Details of the performance and calibration of the microconductivity probe and a description of the towed instrument system is given by Washburn and Gibson (1982a). The towed instrument platform and decoupling system for constant depth tows are further described by Naysmyth (1980) and Gibson (1979).

Washburn and Gibson (1982b) show that the turbulence parameters ϵ, χ, and C in the seasonal thermocline are determined by patches of microstructure activity occupying a small fraction of the total record. In the present paper we examine 33 of the most active patches in detail, occupying about 230 m of the total 5700 m record, or 4%. The patches completely dominate the space average ϵ, χ, and C values for the record; for example, 70% of the mean χ value is accounted for by only 6 active patches occupying only 1% of the total record. In terms of average parameters, none of these "active" patches appear to be actively turbulent at the largest vertical wavelengths at the time of measurement.

Once regions of temperature microstructure activity were identified, raw spectral estimates were obtained by Fourier transforming (FFT algorithm) segments of data within the regions and ensemble averaging spectra from the adjacent segments. Prior to applying the transform, data segments were first differenced for pre-whitening and tapered with a Gaussian window. Typically 10 to 32 spectra were averaged over horizontal distances of 5 to 15 m, depending on the length of activity. Very few patches were found with horizontal extents greater than 10 m.

To provide further smoothing, the ensemble averaged spectra were geometrically band averaged to a maximum of 16 points per frequency band. Following the band averaging the spectra were converted from temporal to spatial frequency using the Taylor hypothesis $\partial/\partial x = -(\partial/\partial t)\, U^{-1}$ and the average velocity U of the instrument platform through the region of activity. Average velocity for each region was obtained from a ducted current meter mounted on the instrument platform.

A final step in the preparation of temperature gradient spectra was a consideration of the effects of limited microconductivity probe frequency response and spatial resolution. As discussed by Washburn and Gibson (1982a) the open flow design of the microconductivity probe results in flushing of the cell averaging volume at the free stream velocity with boundary layer effects confined to a very thin region near the probe surface. This results in very high frequency response compared to most other temperature sensors such as thermistors. Of the two instrumental effects spatial resolution limitation is a more important factor in estimating spectra than the frequency response. Because most of the results of this paper deal with portions of the temperature gradient spectrum at wavelengths many times the probe electrode length, no correction for spatial resolution has been applied. Portions of some conductivity spectra at the highest wavenumbers appear to be dominated by salinity fluctuations which should have the same universal spectral form as the temperature, but displaced to higher wavenumber by a factor of about 30. No substantial departures from the expected spectral form for salinity were observed to the smallest wavelengths presented here; that is, to wavelengths $\lambda = 0.5$cm which is twice the electrode length. A further discussion of the spatial resolution of the microconductivity probe is given by Washburn and Gibson (1982a). Because signal levels in the active microstructure regions examined in this paper were high, none of the data presented have been adjusted for noise.

3. Hydrodynamic Activity Inferred From Temperature Gradient Spectra

Examples of temperature gradient spectra from three regions of microstructure activity in which the spectral peaks have been resolved are shown in Figure 1. The rising spectrum at the bottom of Fig. 1 is an equivalent temperature gradient noise spectrum plotted as a function of wavenumber. The one-dimensional Batchelor spectrum (dashed line) given by Gibson and Schwarz (1963) is superimposed on the upper spectrum. All three spectra are somewhat broader than the Batchelor form, particularly spectrum D-6 which has a very wide spectral maximum. Cox numbers indicated on Fig. 1 are computed from $C = 3\,\overline{(\partial T/\partial x)^2}/(\partial \bar{T}/\partial z)^2$ where isotropy of the small scale temperature fluctuations has been assumed. The mean vertical temperature gradient used in computing C is 0.3 °C/m. This was derived from a salinity-temperature-depth profile of S.P. Hayes (personal communication, 1978) obtained about 1.5 hours before the 7 September tow at the same depth as the average for the tow of 35 m. The general broadening of the spectral maximum with decreasing Cox number apparent in Fig. 1 is a trend found in all of the towed data presented here and agrees qualitatively with the findings of Dillon and Caldwell (1980) in their very detailed comparisons with the Batchelor form. This broadening and apparent departure from the Batchelor form at small Cox number indicates a greater variation of ϵ within regions of weak microstructure activity.

The position of the Batchelor spectrum in wavenumber, or equivalently the peak wavenumber, depends on ϵ within the fluid; a higher value of ϵ results in convective straining of isotherms to smaller scales, thus producing a higher peak wavenumber of the temperature gradient spectrum. The peak wavenumber of the one-dimensional Batchelor spectrum given by Gibson and Schwarz (1963) occurs at radian wavenumber,

$$k_p = \frac{0.43}{\sqrt{q}} \left(\frac{\epsilon}{\nu D^2} \right)^{1/4} \tag{1}$$

where D is the thermal diffusivity of sea water and q is an experimentally determined constant. Recent oceanic measurements by Oakey (1982) using an airfoil shear probe and a platinum film

temperature sensor produced estimates of q in the range $q = 3.7 \pm 1.5$. In this paper we take $q = 2\sqrt{3}$, near the mid-points of the experimentally determined range and at the upper limit of the theoretical estimate of the range of q given by Gibson (1968). This results in estimates of ϵ and rate of strain $\gamma = (\epsilon/\nu)^{1/2}$ which are slightly larger than those computed using the expressions in Gibson (1980) where $q \doteq 2$ was assumed. From (1) it may be seen that large variations of ϵ within an averaging segment will result in the superposition of temperature gradient spectra with differing peak wavenumbers and will produce a composite spectrum with a broader maximum than the Batchelor form.

Strong intermittency of ϵ will also tend to increase the value of q somewhat, as discussed by Gibson (1982b). Although active turbulence is a necessary condition for the initial generation of temperature and salinity microstructure, the Batchelor spectrum will persist even after the microstructure is completely fossil turbulence and all overturning turbulent motions have been damped away, as shown by Gibson (1982b). Physically, the Batchelor spectrum reflects a local equilibrium between molecular diffusion and the fluid rate of strain. High wavenumber Fourier elements of the scalar field tend to align with the local least principle rate of strain axes and are rapidly converted to the Batchelor scale $(D/\gamma)^{1/2}$ where diffusive damping begins. As shown by Gibson (1980), if the rate of strain γ decreases to less than 5N all turbulence will cease, but the convective mixing in the fossil turbulence will continue and the dissipation rate ϵ can still be estimated using (1).

The dissipation rate of scalar variance χ_θ is defined as $2 D_\theta (\nabla \theta)^2$, where D_θ is the molecular diffusivity of a conserved scalar fluid property θ such as temperature or salinity. χ_θ may generally be used as an indicator of hydrodynamic activity. As shown by Gibson (1980), when a patch of turbulence occurs, the maximum vertical extent of the patch will be about $(\epsilon_o/N^3)^{1/2} \equiv L_{Ro}$ where ϵ_o is the dissipation rate of the turbulence at fossilization and N is the ambient Väisälä frequency $(\frac{g}{\rho}\frac{\partial \rho}{\partial z})^{1/2}$. Large vertical overturning scales require large turbulent dissipation rates ϵ. χ_θ increases with large ϵ_o and L_{Ro} if $\nabla \bar{\theta}$ is vertical since larger θ differences are entrained by the larger overturning scales. At fossilization

$$\chi_{\theta o} = \frac{2}{13} (\nabla\bar{\theta})^2 \epsilon_o N^{-2} \tag{2}$$

as shown by Gibson (1980) and Gibson (1982c). From (2) we can express ϵ_o in terms of the Cox number $C_\theta = \overline{(\nabla\theta)^2}/(\nabla\bar{\theta})^2$

$$\epsilon_o = 13\, D_\theta\, C_{\theta o} N^2 \tag{3}$$

using the definition of χ_θ. The actual Cox number C_θ in fossil θ turbulence will be less than the initial value $C_{\theta o}$ because $\gamma < \gamma_o$ and mixing continues. According to (Gibson, 1980)

$$C_\theta \leqslant C_{\theta o}\, (\gamma/\gamma_o)^{2/3} \tag{4}$$

where $\gamma = (\epsilon/\nu)^{1/2}$ is the rate of strain at the time of observation. Therefore, combining (4) and (3) gives

$$\epsilon_o' \equiv 13\, D_\theta\, C_\theta N^2 \leqslant \epsilon_o \tag{5}$$

Equations (1) and (5) provide two independent estimates of the dissipation rate ϵ based on the θ gradient spectrum. If the turbulence of the microstructure is at fossilization the two estimates should be equal. If the microstructure is fossil-θ-turbulence at large scales (or all scales if $\gamma < 5N$) then $\epsilon < \epsilon_o'$. The ratio ϵ/ϵ_o' gives a measure of the degree of turbulence activity. From (1) and (5) with $q \doteq 2$

$$\epsilon/\epsilon_o' = \nu\, D_\theta\, (k_p/0.3)^4/13\; C_\theta N^2 \equiv A_T^2 \tag{6}$$

where A_T is the turbulence activity parameter defined by Gibson (1980). Measured values of A_T for the present microstructure patches are given in the next section with the assumption that $q = 2\sqrt{3}$.

From (3), (4), (5), and (6) and the definitions of χ, C and γ it follows that

$$\chi/\chi_o = C/C_o \leqslant A_T \tag{7}$$

and that

$$\epsilon/\epsilon_o \leqslant A_f^3 \tag{8}$$

as shown by Gibson (1981b). Equality in (4), (7), and (8) occurs for microstructure during and immediately after the completion of the fossilization (turbulence damping) process. Inequality results because the microstructure continues to mix and C decreases by internal wave and nonturbulent restratification motions even after the turbulence has been completely damped away by the stable stratification. In Section 4 estimates of χ_o, C_o, and ϵ_o are made assuming equality in (7) and (8), respectively.

Temperature gradient spectral levels in layers of strong thermal stratification increase with both ϵ and χ. This is illustrated by the relationship between the dissipation rate ϵ_o and Cox number C_o given by (3). Since (as shown by Gibson, 1980)

$$C_o \propto PrRe_o = Pe_o$$

where Pe_o is the Peclet number of the turbulence at fossilization and since in a thermally stratified layer $N^2 = g\alpha(\partial \bar{T}/\partial z)$, where g is gravity and α is the coefficient of thermal expansion, we see from (3) that the velocity gradient variance for the same Reynolds number turbulent patches will tend to increase proportionally with the mean vertical temperature gradient. Thus,

$$\epsilon_o \approx \nu g \alpha \, Re_o \, (\partial \bar{T}/\partial z) \tag{9}$$

where we have assumed $C_o = Pr \, Re_o/13$, corresponding to a critical value of Re_o of about 25 and a critical value of C_o of about $2\,Pr$ (see Gibson, 1982c), and $Pr = \nu/D$. Values of Re_o in the pycnoline will tend to be increased compared to adjacent layers by the concentration of shear due to the vorticity production term $\nabla p \times \nabla \rho$. From (9), ϵ values in the pycnoline

microstructure patches should not only be larger than values in the background fluid of the layer, but also larger than ϵ values in patches from less strongly stratified layers. The largest Re_o value for the present data is 1.8×10^6.

4. Turbulence And Mixing Parameters Within The Most Active Microstructure Patches

Figure 2 shows temperature as a function of horizontal distance for the data records analyzed, as well as the microstructure patch locations. Temperature gradient variance plots, T-S diagrams and other details are given in Washburn and Gibson (1982b) for the same data. Four digital records A, B, C and D were produced from analog tape, for a total of about 5700 m of the 8000 m total record. The individual microstructure patches selected for analysis are numbered in Fig. 2. Table 1 summarizes the statistical parameters computed for each of the numbered patches. The 33 patches were selected to include the regions of strongest temperature gradient variance activity which dominate the total record average $\overline{\chi}$. Because the layer is strongly stratified, the patches should also include the regions which dominate the average viscous dissipation rate $\overline{\epsilon}$. Unlike regions in a fully turbulent mixed layer where strong turbulent mixing could reduce the amplitude of the small scale temperature fluctuations below the noise level of the sensors, strong turbulence in a layer stratified by temperature should invariably be associated with strong temperature fluctuations since as ϵ increases the vertical scale of entrainment and thus the range of temperature difference both increase. This is shown by (9) and the discussion in Section 3.

As shown in Table 1, the patches vary in length from 3.8 to 15 meters and cover a depth range from 31.3 to 37.1 meters. Cox numbers C for the patches are between 241 and 4009. The ratio γ/N was greater than the critical value of 5 indicating turbulence for only 11 of the 33 patches, with maximum value of about 16 corresponding to a maximum ϵ value of $1.5 \times 10^{-3}\text{cm}^2/\text{s}^3$. The other 22 microstructure patches were nonturbulent with minimum γ/N values as low as 0.3 comparable to γ/N for deep ocean internal waves obeying the Garrett and Munk spectrum, and with minimum ϵ values of $(3-5) \times 10^{-7}\ \text{cm}^2/\text{s}^3$. Since these γ/N values are derived from the wavenumber k_p at the temperature gradient spectral peak using (1), they will tend to be smaller than values estimated from a higher wavenumber fit if the spectrum is broadened by variations in ϵ within the patch.

Temperature dissipation rates χ_T in the patches ranged from 6.1×10^{-6} °C^2/s to 1.0×10^{-4} °C^2/s for the most active patch D-4 which also had the largest Cox number of 4009. The weighted average

$$\bar{\chi} = \sum_{i=1}^{33} (\Delta x_i \chi_i / L) = 1.02 \times 10^{-6} \text{ °C}^2/\text{s}$$

where $L = 5700$m is the total record length and Δx_i is the length of the i-th patch. $\bar{\chi}$ is a lower bound of the actual space average, since χ outside the patches has been neglected. Including the background variance, which is mostly noise, increases $\bar{\chi}$ by less than 30%. Neglecting all but the six most active patches, comprising only 0.8% of the total record, decreases $\bar{\chi}$ by only 30%. $\bar{\chi}$ estimated above is only 10% less than the mean of the lognormal probability density function derived for these data in Washburn and Gibson (1982b).

Similarly, the weighted average viscous dissipation rate for the record was computed to be $\bar{\epsilon} = 2.0 \times 10^{-5}$cm^2/s^3, setting $\epsilon = 0$ outside the patches. If the background ϵ is less than or equal to the smallest ϵ value observed in a patch, then $\bar{\epsilon}$ will increase by less than 1%. Since temperature gradient spectra for the background regions were not resolved, it is not possible to estimate the uncertainty in this calculation based on measurements. From (3), it seems likely that ϵ values will be maximum in the patches of maximum χ value and that the intermittency of ϵ will be comparable to the intermittency of χ, so that $\bar{\epsilon}$ will be a lower bound of the space average. Minimum values of ϵ for the patches were $(3-5) \times 10^{-7}$cm^2/s^3, which is less than the ϵ noise level for available velocity sensors by at least a factor of ten. ϵ values outside the patches are probably even lower.

Preliminary values of the salinity dissipation rate χ_S are also listed in Table 1. These are derived by fitting viscous convective subranges $\phi_S = q\, \chi_S\, k^{-1}\, \gamma^{-1}$ to high wavenumber portions of some of the conductivity spectra which departed from a strong temperature spectrum rolloff at levels significantly above the noise spectrum. Since

$$\phi_S = (\partial S/\partial\sigma)^2\phi_{\sigma S} \text{ and } \phi_T = (\partial T/\partial\sigma)^2\phi_{\sigma T}$$

where $\phi_{\sigma S}$ and $\phi_{\sigma T}$ are the salinity and temperature components of the conductivity spectrum, then

$$\phi_S = (\partial S/\partial\sigma)^2(\partial T/\partial\sigma)^{-2}\,(\phi_{\sigma S}/\phi_{\sigma T})\,\phi_T = 0.81\,(\phi_{\sigma S}/\phi_{\sigma T})\phi_T$$

where S is in (‰) and T is in °C. The partial derivatives $\partial S/\partial\sigma$ and $\partial T/\partial\sigma$ are obtained from the salinity scale of Lewis (1980) as discussed by Washburn and Gibson (1982b). Since the effective rate of strain γ in the microstructure patches is the same for both temperature and salinity, the salinity variance dissipation rate in $(‰)^2s^{-1}$ may be estimated as

$$\chi_S = 0.81\,\chi_T(\phi_{\sigma S}/\phi_{\sigma T}) \tag{10}$$

where $(\phi_{\sigma S}/\phi_{\sigma T})$ is the ratio of viscous convective subranges of the conductivity spectra ϕ_σ attributed to salinity and temperature, respectively, and χ_T is in $°C^2/s$. The method is illustrated in Figure 3, which shows spectra from patch 1 and 4 of record A compared to the noise spectrum. The spectrum from patch A-4 shows a clear departure from the temperature diffusive rolloff beginning at k=1 cpcm at a level a factor of 7 above the noise. The ratio $\phi_{\sigma T}/\phi_{\sigma S}$ is about 60 $°C^2/(‰)^2$. Since χ_T for patch A-4 is 1.7×10^{-5} $°C^2/s$ then $\chi_S = 2.2 \times 10^{-7}$ $(‰)^2/s$, as listed in Table 1. No salinity viscous convective subrange above the noise is shown in Fig. 3 for patch A-1, so χ_S must be $< 2.2 \times 10^{-7}$ $(‰)^2/s$, computed by the same method.

If the vertical eddy diffusivities of temperature and salinity are equal then one would expect

$$\chi_S/\chi_T = \left[(\partial\bar{S}/\partial z)/(\partial\bar{T}/\partial z)\right]^2 \tag{11}$$

from the Osborn and Cox (1972) model. For the present data $\left[(\partial\bar{S}/\partial z)/(\partial\bar{T}/\partial z)\right]^2$ is about

(1/400) $[(‰)/°C]^2$, which is smaller than most of the χ_S/χ_T ratios found from Table 1, but larger than others, indicating that to first order $K_S \approx K_T$. Salinity Cox numbers are not listed in Table 1 but may be readily computed. For example, for patch A-4

$C_S = \chi_S/2D_S(\partial\bar{S}/\partial z)^2 = 5 \times 10^5$.

Figure 4 is a comparison of ϵ values measured in the seasonal thermocline during MILE by different techniques. The present towed body inferred values of ϵ, ϵ'_o and ϵ_o for the microstructure patches listed in Table 1 are shown as numbered squares, points and crossed squares, respectively, with the three record depths A, B and D shown at the right. Values from record C are not shown but are given in Table 1. Patch dissipation rates of Dillon and Caldwell (1980) are shown as circles and triangles for low and high wind speeds, respectively, and the ϵ profiles presented by Lange (1981) are shown by lines. Lange's ϵ values were measured using a heated thermistor on the VMSR dropsonde.

All measurements were made during a six day period from September 1-7 (Julian Day 244-250). Wind speeds for both dropsonde data sets spanned the 7.7 m/s winds of September 7 (JD 250) for the present towed body measurements. The temperature profile on JD 246 by Lange shows the seasonal thermocline was at 30-40 m with $d\bar{T}/dz \sim 0.3$ $°C/m$, the same stratification condition indicated by S. P. Hayes (personal communication, 1978) on JD 250. On JD 245 Lange (1981) shows the maximum thermocline gradient was the same strength but a few meters shallower. Dillon and Caldwell (1980) show temperature profiles for their low wind speed (5.5 m/s) and high wind speed (15.5 m/s) which have $\partial\bar{T}/\partial Z$ values close to 0.3 °C/m in the depth range 30-40 m. Thus it appears that the oceanographic and meterological conditions for the three data sets are reasonably well matched so that the mixing processes in the seasonal thermocline should be comparable.

As discussed previously, the criterion for the existance of active turbulence in terms of the range of possible overturning wavelengths λ is that $1.2\,L_R \geqslant \lambda \geqslant 15\,L_K$. The buoyancy wavelength $1.2\,L_R$ and the viscous wavelength $15\,L_K$ are plotted at the top of Fig. 4 as a function of ϵ for the seasonal thermocline with $\partial\bar{T}/\partial Z = 0.3$ $°C/m$, $N = 2.3 \times 10^{-2}$ rad/s. Active

turbulence can exist only for ϵ values greater than about 10^{-4} cm^2s^{-3}, corresponding to the point in Fig. 4 where the 1.2 L_R and 15 L_K lines cross. The range of actively turbulent wavelengths is shown by the diagonally hatched region on the right. Any microstructure patches to the left of the diagonally hatched region must be completely fossil turbulence, since buoyancy and viscous forces dominate motions at all scales of the microstructure. This diagram neglects the known variations of ϵ and N within the patch, which will probably always permit some local turbulence.

Most of ϵ samples shown in the lower portion of Fig. 4 appear to be nonturbulent, except for a few towed body patches (33% of the total) and some of the Dillon and Caldwell (1980) microstructure patches at high wind speeds. Most of the tow body and the Dillon and Caldwell (1980) dropsonde ϵ values for low winds were at about 10^{-5} cm^2s^{-3}.

Values of $\epsilon_o = 13\ D\ C_o\ N^2$ for the towed body microstructure patches are generally higher than even the Dillon and Caldwell patch values for high winds, with a maximum value of 2.8 cm^2s^{-3} for patch D-4. The range of ϵ values, past and present, spans over 7 decades and illustrates the extreme intermittency of the turbulence in space and time.

Surprisingly, the Lange (1981) ϵ profiles lie at the upper end of the range $10^{-4} - 10^{-3}$ cm^2s^{-3} of patch ϵ values from Dillon and Caldwell (1980) and the present towed body patch ϵ values. Since the continuous VMSR ϵ profiles should represent non-patch "background" fluid about 95% of the time, it might be expected that the profiles would show ϵ values less than or equal to the minimum ϵ values estimated in the microstructure patches; that is, as low as $10^{-7}cm^2s^{-3}$ or factors $10^3 - 10^4$ less than observed by Lange (1981). Lange (1981) estimates an rms noise of less than $4 \times 10^{-3}\ s^{-1}$ in $\partial w/\partial z$, the vertical velocity gradient in the vertical direction, which gives ϵ noise $\leqslant 2 \times 10^{-6} cm^2s^{-3}$. A temperature gradient sensitivity of $8 \times 10^{-3} m/s$ °C is given, corresponding to a temperature induced ϵ of

$$\epsilon_T = (15/6)\ (\nu/d)\ (0.8)^2 \chi cm^2s^{-2} = 16\chi\ cm^2s^{-3}$$

where χ is in $°C^2/s$. Since Lange (1981) reports χ profiles in the seasonal thermocline of only

10^{-8} °C^2/s, the temperature noise should be only 1.6×10^{-7}cm$^2 s^{-3}$, much less than the observed values. It seems physically unrealistic that background ϵ values should be (2-3) orders of magnitude greater than the minimum ϵ values in the microstructure patches and comparable to maximum ϵ values in the patches. Consequently, we conclude that the VMSR noise level may have been underestimated or that temperature effects may be more important. Most profiles of ϵ in the seasonal thermocline in other ocean regions by Gargett and Osborn (1981) using the airfoil shear probe show • values of less than 10^{-6}cm$^2 s^{-3}$ (the instrument noise level), which is consistent with our observations.

Figure 5 shows an intercomparison of χ and C values in the seasonal thermocline estimated and measured by different techniques. Towed body χ and C values from Table 1 are shown as numbered open squares and χ_o and C_o values as numbered crossed squares. The record designation and approximate depth range for the towed data are shown at the right. Dillon and Caldwell (1980) C values for light and strong winds are given by circles and triangles, as in Fig. 4. Since the mean temperature gradient for the Dillon and Caldwell (1980) data was $\approx 0.3\,°C\,m^{-1}$ the χ scale should also be approximately correct for inferring χ values from their values of C. The wind speed for the towed body data was about 7.7 m s^{-1}, which is intermediate to the 5.5 m s^{-1} and 15.5 m s^{-1} wind speeds for the Dillon and Caldwell (1980) data.

As shown in Fig. 5, the low and high wind speed χ values of Dillon and Caldwell (1980) have the same minimum, about 10^{-7} °C^2/s, but the high wind values extend to maximum values over 2×10^{-4} °C^2/s compared to only 10^{-6} °C^2/s for low winds. The towed body patches, with intermediate wind speeds, generally have intermediate χ values, ranging from 4×10^{-6} to 1.0×10^{-4} °C^2/s, which is in very satisfactory agreement. However, the wind speed on 7 September is closer to the lighter wind value of Dillon and Caldwell (1980) while the upper limit of the χ range from 7 September approaches the highest χ values they observed during the higher winds. The estimated space average $\bar{\chi} = 1.0 \times 10^{-6}$ °C^2/s for the towed body data also seems to be intermediate between the space averages which might be estimated for the Dillon and Caldwell (1980) dropsonde data at different wind speeds, but as mentioned

previously, Dillon and Caldwell (1980) did not make such estimates of mean values for this depth range because of the high intermittency of their sample values.

In contrast to both the towed body and Dillon and Caldwell (1980) patch χ values, the Lange (1981) χ profiles for intermediate wind speed ranges are in a substantially lower range, from 10^{-9} to 10^{-8} °C^2/s. This is somewhat higher than the mode $\chi_{MODE} = 4 \times 10^{-10}$ °C^2/s of the lognormal χ probability density function measured by Washburn and Gibson (1982b). χ_{MEAN} was 1.1×10^{-6} °C^2/s for the same distribution. Clearly as a measure of the space average mean $\bar{\chi}$ the Lange (1981) vertical χ profiles are subject to large undersampling error, and are a factor of $10^2 - 10^3$ too small. This is consistent with the interpretations proposed by Gibson (1982a,b) that the Gregg (1977) dropsonde estimate of $\bar{\chi}$ in the main thermocline and the Oakey (1980) estimate of $\bar{C}$ in the Denmark Strait, respectively, are both too small by factors of at least 10^2 due to undersampling error. It is also consistent with the proposal of Gibson (1980, 1981a) that the Gregg (1976) and Osborn and Bilodeau (1980) estimates of $\bar{\chi}$ and the Crawford (1976) and Crawford and Osborn (1980) estimates of $\bar{\epsilon}$ in equatorial undercurrent core layers may be too small by even larger factors. Large underestimates of χ and ϵ mean values due to undersampling error appears to be a characteristic result for single dropsonde turbulence profiles, particularly in ocean layers with strong intermittency. Since the dominant mixing activity may concentrate in layers with strong stratification and strong intermittency, dropsonde turbulence profiles must be used with caution. Individual profiles should not be interpreted as representative of mean values at any depth. Qualitative variations of activity in isolated profiles may only reflect vertical variations of turbulence intermittency with consequent variations in undersampling error, so that the profiles will actually tend to be negatively correlated with true mean turbulence dissipation rates. It should be pointed out that Lange (1981) emphasizes that the number of ϵ and χ profiles he presents is small and that the 'statistical stability' of his inferred mixing 'scenarios' is a problem. Lange (personal communication, 1982) found some profiles in the seasonal thermocline with χ values larger than 10^{-6} °C^2/s, but did not report these in Lange (1981).

Figure 6 shows the turbulence activity parameter A_T as a function of C for the microstructure patches from records A, B and D of Table 1. Most of the patches are in the completely fossil turbulence portion of the diagram, with $\gamma < 5N$. Rather than a constant value of $A_T = 0.18$ as required by the universal scaling proposed by Caldwell et al. (1980), A_T ranges between less than 10^{-2} to about 0.8. A line representing A_T values computed from the Caldwell et al. (1980) measurements is shown in Fig. 6, as discussed by Gibson (1982c). Also shown is a dashed line of slope +1 corresponding to equality in (7), with $A_T = C/C_o$ extrapolated to $A_T = 1$, giving a lower bound estimate of the Cox number of patch D-4 at fossilization of $C_o \geqslant 3 \times 10^5$. The actual trajectory in time for patch D-4 should be in the opposite direction starting from a point in the turbulence range to the right and perhaps slightly above the point $(A_T, C) = (1, 3 \times 10^5)$ and proceeding downward on a curved path to the point in the fossil region actually measured, at $(1.2 \times 10^{-2}, 4009)$.

Besides undersampling errors of the space averages due to spatial patchiness, the large $\bar{\chi}_o$ values in Fig. 5 and large $\bar{\epsilon}_o$ values in Fig. 4 show that the estimates $\bar{\chi}$ and $\bar{\epsilon}$ may be subject to large undersampling errors due to time intermittency of the turbulence process when used as measures of the space-time averages $<\chi>$ and $<\epsilon>$. Presumably

$$\bar{\chi} < <\chi> < \bar{\chi}_o$$

and

$$\bar{\epsilon} < <\epsilon> < \bar{\epsilon}_o$$

where the space-time averages are over time periods less than the age of the patch with largest C_o value, in this case patch D-4. More studies of the evolution of fossil turbulence with time are required before $<\chi>$ and $<\epsilon>$ can be estimated with any confidence from fossil turbulence evidence alone.

Figure 7 shows a comparison between the quantity ϵ'_o from (5) and the quantity

$$\epsilon''_o \equiv L''^2_T N^3 \tag{12}$$

$$L''_T \equiv 2\overline{(\delta T)^2}^{1/2}/(\partial \bar{T}/\partial z) \tag{13}$$

where the length scale L''_T is computed from the band passed temperature variance $\overline{(\delta T)^2}$ and the mean temperature gradient. L''_T represents an overturning length scale similar to but smaller than the Thorpe overturning scale $L_T \equiv \zeta_{max}$ defined by Gibson (1982a) since $\epsilon_o' \approx \epsilon_o''$ is smaller than ϵ_o. The scale in (13) was also used by Stillinger (1981) as an estimator of the vertical overturning scale which produced the density fluctuations observed in his stratified water tunnel experiments. A correlation between ϵ'_o and ϵ''_o might be expected since both are estimators of previous dissipation rates: ϵ'_o is the dissipation rate required to produce the observed Cox numbers while ϵ''_o is the dissipation rate required to produce overturning on vertical scales L''_T. Both dissipation estimates are consistently less than ϵ_o because both δT_{rms} and C on which they are based have decreased due to mixing between the time the events were most active and the time at which they were observed. Because horizontal temperature spectra tend to be steeply sloping with the greatest contributions to the variance arising from the longest wavelengths resolved, we estimate δT_{rms} in L''_T from wavelengths 0.5 m to 1 cm. Temperature variance in this band as found to be a good indicator of microstructure activity as discussed below. In estimating temperature variance from this band it is assumed that fluctuations at wavelengths of 0.5 m and smaller within microstructure patches are produced by turbulence. If contributions to $\overline{(\delta T)^2}$ used in evaluating L''_T include low wavenumber components which are much larger than patch sizes (wavelengths of several meters and larger) arising from the internal wave field say, this interpretation is invalid. The correlation between ϵ'_o and ϵ''_o is quite good, with deviations generally less than a factor of two either way. Measurements of ϵ''_o are intrinsically much easier than ϵ'_o because ϵ'_o requires frequency response to the diffusive cutoff of the temperature gradient spectrum at wavelengths about 1 cm, whereas an adequate estimate of ϵ_o'' could be obtained by detecting temperature fluctuations with wavelengths of about 50 cm. Generally we would expect $\epsilon_o \geqslant \epsilon''_o \geqslant \epsilon'_o$.

Figure 8 shows a comparison between $\overline{(\delta T)^2}$ and $\overline{(\partial T/\partial x)^2}$ estimated for wavelengths

from 50 cm to 1 cm for a 400 m section of temperature record containing patch D-4 (see Figure 2). The traces are qualitatively very similar and produce the correlation between ϵ'_o and ϵ''_o shown in Fig. 7. A correlation between $(\delta T)^2$ and $(\partial T/\partial x)^2$ similar to that shown in Fig. 8 was also found if variance was computed for the range of wavelengths 100 to 1 cm. Figure 9 shows temperature spectra and temperature gradient spectra plotted in variance preserving form from patch D-4, illustrating the separation in wavenumber between the portions of the temperature spectrum which dominate the two measures of turbulence dissipation rates at fossilization ϵ'_o and ϵ''_o. Most of the variance $\overline{(\delta T)^2}$ is determined by wavelengths larger than 10 cm while most of the variance $\overline{(\partial T/\partial x)^2}$ is determined by wavelengths smaller than 10 cm. Figure 10 compares $A_T^2 \equiv \epsilon/\epsilon'_o$ from (5) with ϵ/ϵ''_o for the 33 patches of Table 1. The clustering of the points about the line with slope +1 suggests that the two parameters are nearly equivalent over the full range of ϵ/ϵ'_o values from 6×10^{-5} to 0.61. The slight displacement of the points up from the +1 line at very small values of the parameters may be due to molecular diffusion. Small values of ϵ/ϵ'_o and ϵ/ϵ''_o imply that the microstructure is "old" so that the Cox number appearing in the denominator of $\epsilon/\epsilon'_o = \epsilon/13\mathrm{DCN}^2$ may be reduced as molecular diffusion erases the high wavenumber contributions which dominate $\overline{(\nabla T)^2}$. The rms temperature fluctuation of L''_T in the parameter $\epsilon/L''^2_T N^3$ is dominated by lower wavenumber contributions which take much longer to be affected by diffusion with the result that $\epsilon/13\mathrm{DCN}^2$ may be larger than $\epsilon/L''^2_T N^3$ after long times. At this time no technique is available to measure $\bullet$ without direct measurements of either $\partial u/\partial x$ or $\partial T/\partial x$ with spatial resolution to the viscous or diffusive scales.

Finally, since much of this paper deals with quantities which must be derived indirectly, a discussion of possible error sources and uncertainties is in order. From (1) ϵ depends on the fourth power of the peak wavenumber k_p, and since k_p must be determined from a broad spectral maximum in some cases ϵ may be quite uncertain, partly due to errors and partly reflecting the actual broad range of ϵ values which causes the broad spectral maximum in the first place. The uncertainty in ϵ due to errors is generally much less than the range of ϵ variations. To

reduce scatter, spectral points near the peak wavenumber and higher wavenumbers are heavily smoothed prior to estimating k_p. Attenuation of high wavenumber components of $\overline{(\nabla T)^2}$ due to spatial resolution limitations of the microconductivity probe may result in underestimates of the Cox number by as much as 40% in the worst case although in most regions spectra are probably well resolved. This uncertainty is usually small compared to the wide range of C and χ variations. Noise in temperature gradient spectra tends to increase with frequency which results in overestimates of the Cox number. Subtraction of noise spectra from signal spectra decreases Cox number estimates up to 30% in some regions with lower spectral levels but for most regions the differences are far less. High wavenumber portions of the conductivity gradient spectra which are apparently due to salinity fluctuations in some cases are affected by spatial resolution limitation of the probe. For this reason no region was found in which the diffusive scale salinity gradient variance $\overline{(\partial S/\partial x)^2}$ could be resolved. However, the break point in the conductivity gradient spectra used in making preliminary estimates of χ_S usually occurred at scales of 1 cm and greater or at least 4 times the probe electrode length. At these scales the probe attenuation is probably not too severe.

The primary conclusions of the present paper are not affected by uncertainties in ϵ and χ values as small as $\pm$ 40%. From Figures 4 and 5 we see that the range in measurement values of ϵ is over 4 decades and the range of measured χ values is over 5 decades. Agreement between the towed body and the Dillon and Caldwell (1980) patch χ and ϵ values is quite independent of the uncertainty in calculations of individual patch values.

Measurement uncertainties are generally less than theoretical uncertainties in the expressions used to estimate previous turbulence dissipation rates and space-time averages. Gibson (1982a) estimates the uncertainties in the various fossil turbulence expressions reviewed in Section 3, giving $\epsilon_o = (13 \pm 2) D_o N^2$ for (3) and $\gamma_{min} = (5 \pm 1) N$ or $(1.2 \pm 0.2) L_R \geqslant \lambda \geqslant (15 \pm 3) L_K$ for the uncertainty in the present turbulence criteria.

The estimates of previous ϵ_o, χ_o and C_o values at fossilization using (7) and (8) give lower bounds. The uncertainty of the lower bound depends on $A_T \equiv \sqrt{\epsilon/\epsilon'_o}$. ϵ measured using the temperature gradient technique is generally uncertain by about $\pm 30\%$ if the spectrum approximates the Batchelor form, but as discussed previously, spectra are often broadened by averaging over patches which contain wide variations in ϵ. For these patches various procedures might be selected to chose a representative value. In this paper we have chosen ϵ corresponding to k_p, the wavenumber at the spectral peak, using (1). Some of the patch fluid, possibly most of the patch fluid, will have ϵ values near ϵ_p found by this method. ϵ_p will tend to be less, sometimes orders of magnitude less, than ϵ_B estimated from a point a decade below the peak using Dillon and Caldwell's procedure. For example for the most active patch D-4 the spectrum peaks at a wavenumber k_p 9.6 times less than the wavenumber k_B where the spectrum is a decade below the peak, compared to 3.7 times less for the 1-D Batchelor spectrum in Fig. 1. Therefore ϵ_B is 45 times ϵ_p, γ_B is 6.7 $\gamma_p = 6.7N$ and A_T increases from 1.2×10^{-2} to 8.0×10^{-2} which is slightly inside the region of mixed active and fossil turbulence in Fig. 6. The Caldwell *et al.* (1980), Dillon and Caldwell (1980) and Dillon (1982a) A_T values from MILE are maxima, and many would be shifted into the completely fossil range (Fig. 6) if they had been based on ϵ_p rather than ϵ_B. Only a half dozen patches for MILE reported by Dillon (1982a) have A_T values in the completely fossil range with $\gamma < 5N$, and these are always patches with small C values in the range 25-210; most A_T values are in the mixed active and fossil range with $A_T \approx 0.2$ (Fig. 6), and only one patch was found with $A_T = 1.27$ indicating completely active turbulence ($\gamma/N = 85$, $C = 3000$, depth = 17 m). The experimental results of the OSU dropsonde measurements are therefore quite consistent with our towed body result. Because the largest ϵ estimates for both data sets are generally several orders of magnitude less than the smallest estimates of ϵ_o values required for completely active turbulence, the conclusion that at least the largest scale temperature fluctuations of the microstructure patches are "fossil turbulence" remnants of previous, stronger turbulence activity seems inescapable.

The space-time average dissipation rates $<\epsilon>$ and $<\chi>$ in the seasonal thermocline can be given lower bounds $\bar{\epsilon}$ and $\bar{\chi}$ and upper bounds $\bar{\epsilon}_o$ and $\bar{\chi}_o$. The lower bound space averages are probably valid over the 25 km scale of the MILE array within about $\pm$ 50% by comparing average values from Table 1 computed over various record lengths. The upper bounds of the space time average depend on the unknown time period that the fossil patches can preserve information about previous ϵ_o and χ_o values. Clearly studies of the time evolution of fossil turbulence patches in the ocean are needed in order to reliably infer space-time average turbulence and mixing parameters from data records of limited space-time duration.

5. CONCLUSIONS

Evidence is presented by Washburn and Gibson (1982b) that the dominant mixing activity in the upper ocean layers during MILE may be concentrated at the depth of maximum vertical density gradient in the seasonal thermocline, at depths 30-40 m. In this paper, detailed analysis of the most active patches of temperature microstructure found in the seasonal thermocline from 5700 m of record is presented. Several conclusions about the mixing processes and the problems of quantitative sampling of the turbulence and mixing activity may be drawn.

First of all, the turbulent mixing is completely dominated by a very small portion of the layer, less than 1% of the record accounting for over 70% of $\overline{\chi}$. This patchiness in space has been noted by previous investigators, and complicates the problem of estimating the actual average values of the turbulence dissipation rates ϵ and χ. Very large record lengths are required for the space averages to converge. Averages from short record lengths are strongly biased to small values. Gibson (1980; 1981a; 1982a,b,c) has suggested that several attempts to estimate mean dissipation rates and vertical diffusivities from a few dropsonde profiles may be biased by factors of $10^2 - 10^4$ to small values by such undersampling errors. Because undersampling error increases with turbulence intermittency and because the intermittency may be largest in the most actively turbulent layers which are the most strongly stratified, it was suggested that the qualitative distribution of ϵ and χ from such dropsonde profiles may be negatively correlated with the profiles of actual mean values. The present intercomparisons between towed body and dropsonde ϵ and χ values seems to confirm these suggestions.

Besides being patchy in space, the mixing process is quite intermittent in time. The space average temperature variance dissipation rate for the present measurements is dominated by the mixing in a few almost completely nonturbulent fossil turbulence patches. Previous χ values in these patches were up to 100 times greater when the patches were actively turbulent according to comparisons with the Gibson (1980) fossil turbulence model. If all the patches detected were simultaneously turbulent with their previous dissipation rates at fossilization ϵ_o and χ_o, the space average ϵ would increase from the measured value of $\overline{\epsilon} = 2 \times 10^{-5} \mathrm{cm}^2 s^{-3}$ to

$\bar{\epsilon}_o = 1.3 \times 10^{-2} cm^2 s^{-3}$ and $\bar{\chi}$ would increase from 1.0×10^{-6} $°C^2 s^{-1}$ to $\bar{\chi}_o = 3.2 \times 10^{-5}$ $°C^2$ s^{-1}, factors of 650 and 32, respectively. Actual space-time averages $<\epsilon>$ and $<\chi>$ should lie somewhere between these bounds; that is, $(\bar{\epsilon},\bar{\chi}) < (<\epsilon>,<\chi>) < (\bar{\epsilon}_o,\bar{\chi}_o)$. These values represent the first attempt to estimate space time average dissipation rates using the Gibson (1980) fossil turbulence model. Several aspects of the attempt are complicated by the large variability of ϵ within the microstructure patches indicated by broadening of spectra compared to the universal Batchelor form. Because ϵ and N are variable small scale turbulence may exist in all the microstructure patches examined even where $\bar{\gamma}/\bar{N} < 5$. However we believe that the evidence for fossil turbulence effects at the largest vertical scales of the microstructure is overwhelming. Dillon (1982a,b) questions this interpretation based on energetic and temperature variance balances which we think are not inconsistent with fossil turbulence. Further discussion of the theoretical issues is beyond the scope of the present paper.

Some preliminary values of salinity dissipation rates χ_S were estimated from high wavenumber portions of the microconductivity spectra which showed salinity viscous convective subranges above the noise. A first order estimate of the vertical diffisuvity ratio K_S/K_T is about 1.0, based on the observation that $\chi_S/\chi_T \approx (\partial\bar{S}/\partial z)^2/(\partial\bar{T}/\partial z)^2$.

Finally, a technique was investigated for detecting $\epsilon'_o = 13DCN^2$ by measuring band passed temperature variance at wavelengths of about 50 cm and smaller rather than the diffusive scale temperature gradient variance. It was found that $\epsilon''_o = [2\delta T_{rms}/(\partial\bar{T}/\partial z)]^2 N^3$ was within a factor of 2 of ϵ'_o for most of the 33 microstructure patches studied, suggesting that rapid surveys of $C \cong (4/13)\,[\delta T_{rms}/(\partial\bar{T}/\partial z)]^2\,(N/D)$ could be carried out with temperature sensors capable of detecting temperature fluctuations at wavelengths of only 50 cm rather than the more demanding centimeter scale resolution required for full resolution of the smallest scale temperature gradients. If our interpretation of the turbulence sampling problem is correct, rapid surveys covering very large areas and depth ranges are likely to be necessary aspects of future ocean turbulence sampling schemes.

Acknowledgements

The authors are grateful to several colleagues for helpful advice and in some cases major assistance without which the present study would have never occurred. Carl Friehe made key contributions to the final preparation of the UCSD MILE equipment and John Schedvin went to sea and took the data. Clayton Paulson should be thanked for his leading role in organizing the Mixed Layer Experiment (MILE), bringing together previously scattered microstructure measurement techniques for the first time and making the present intercomparison possible. We thank Tom Dillon for providing us Dillon (1982a,b) in preprint form.

Initial funding was provided by ONR, much of the data analysis was supported by NSF ENG 27398 (CAL TECH 28-464865), and the final analysis and manuscript preparation was supported by a grant from the UCSD committee on Research.

References

Batchelor, G.K., Small scale variation of convected quantities like temperature in turbulent fluid, Journal of Fluid Mechanics, 5, 113-133, 1959.

Belyaev, V.S., M.M. Lubimtzev, and R.V. Ozmidov, The rate of dissipation of turbulent energy in the upper layer of the ocean, Journal of Physical Oceanography, 5, 499-505, 1975.

Caldwell, D. R., T.M. Dillon, J.M. Brubaker, P.A. Newberger, and C.A. Paulson, The scaling of vertical temperature gradient spectra, Journal of Geophysical Research, 85, C4, 1917-1924, 1980.

Crawford, W.R., Turbulent energy dissipation in the Atlantic Equatorial Undercurrent, Ph.D. Dissertation, University of British Columbia, 1976.

Crawford, W.R. and Osborn, T.R., Microstructure measurements in the Atlantic Equatorial Undercurrent during GATE, Walter Düing, Ed., Pergamon Press, New York, 285-308, 1980.

Davis, R.E., R. deSzoeke, D. Halpern, and P. Niiler, Variability in the upper ocean during MILE. Parts I and II, Deep-Sea Research, 28A, 12, 1427-1475, 1981a,b.

Dillon, T.M., Vertical overturns: a comparison of Thorpe and Ozmidov length scales, Journal of Physical Oceanography, in press, 1982a.

Dillon, T.M., The energetics of overturning structures: implications for the theory of fossil turbulence, Journal of Geophysical Research, submitted, 1982b.

Dillon, T.M., and D.R. Caldwell, the Batchelor spectrum and dissipation in the upper ocean, Journal of Geophysical Research, 85, C4, 1910-1916, 1980.

Gargett, A.E., and T.R. Osborn, Small-scale shear measurements during the fine and microstructure experiment, Journal of Geophysical Research, 86, C3, 1929-1944, 1981.

Gibson, C.H., and W.H. Schwarz, The universal equilibrium spectra of turbulent velocity and scalar fields, Journal of Fluid Mechanics, 16, 365-384, 1963.

Gibson, C.H., Finestructure of scalar fields mixed by turbulence, 1, 2, Physics of Fluids, 11, 2305-2327, 1968.

Gibson, C.H. Apparatus for towing an underwater instrumentation package. United States Patent 4, 175, 432, 11/1979, 1979.

Gibson, C.H., Fossil temperature, salinity, and temperature turbulence in the ocean, in *Marine Turbulence*, J.C.J. Nihoul, Ed., Elsevier, 221-257, 1980.

Gibson, C.H., Buoyancy effects in turbulent mixing: sampling turbulence in the stratified ocean, American Institute of Aeronautics and Astronautics Journal, 19, 1394-1400, 1981a.

Gibson, C.H., Fossil turbulence and internal waves, in *American Institute of Physics Conference Proceedings No. 76: Nonlinear Properties of Internal Waves*, Bruce West, Ed., 159-179, 1981b.

Gibson, C.H., Alternative interpretations for microstructure patches in the thermocline, Journal of Physical Oceanography, 12, 374-383, 1982a.

Gibson, C.H., Fossil turbulence in the Denmark Strait, Journal of Geophysical Research, 87, C10, 8039-8046, 1982b.

Gibson, C.H., On the scaling of vertical temperature gradient spectra, Journal of Geophysical Research, 87, C10, 8031-8038, 1982c.

Gregg, M.C., Temperature and Salinity Microstructure in the Pacific Equatorial Undercurrent, Journal of Geophysical Research, 81, 1180-1196, 1976.

Gregg, M.C., Variations in the intensity of small-scale mixing in the main thermocline, Journal of Physical Oceanography, 7, 436-454, 1977.

Gregg, M.C., Microstructure patches in the thermocline, Journal of Physical Oceanography, 10, 915-943, 1980.

Lange, R.E., Observations of Near-surfacce oceanic velocity strain-rate variability during and after storm events, Journal of Physical Oceanography, 11, 1272-1279, 1981.

Lewis, L.L., the practical salinity scale 1978 and its antecedents, IEEE Journal of Oceanic Engineering, OE-5, 1, 1980.

Naysmyth, P.W., Techniques of measurement from towed vehicles and submersibles, *Instruments and Methods in Air Sea Interaction*, R. Davis, L. Hasse, and F. Dobson, Editors, Plenum Press, 1980.

Oakey, N.S., Detection of the rate of dissipation for small scale velocity and temperature from microstructure measurements, Journal of Physical Oceanography, 12, 256-271, 1982.

Osborn, T.R., Estimates of the Local Rate of Vertical Diffusion from Dissipation Measurements, Journal of Physical Oceanography, 10, 83-89, 1980.

Osborn, T.R. and Bilodeau, L.E., Temperature Microstructure in the Equatorial Atlantic, Journal of Physical Oceanography, 10, 66-82, 1980.

Osborn, T.R., and C.S. Cox, Oceanic finestructure, Geophysical Fluid Dynamics, 3, 321-345, 1972.

Schedvin, J.C., Microscale measurements of temperature in the upper ocean from a towed body, Ph.D. thesis, University of California at San Diego, La Jolla, Ca. 1979.

Stillinger, D.C., An experimental study of the transition of grid generated turbulence to internal waves in a salt-stratified water channel, Ph.D. thesis, University of California at San Diego, La Jolla, Ca. 1981.

Washburn, L. and C.H. Gibson, Measurement of ocean temperature microstructure using a small conductivity sensor, Journal of Geophysical Research, 87, no. C6, 4230-4240, 1982a.

Washburn, L. and C.H. Gibson, Horizontal variability of temperature microstructure at the base of a mixed layer during MILE, submitted to Journal of Geophysical Research, 1982b.

Weinstock, J., Vertical turbulent diffusion in a stably stratified fluid, Journal of Atmospheric Sciences, 35, 1022-1027, 1978.

Williams, R.B. and C.H. Gibson, Direct measurement of turbulence in the Pacific equatorial undercurrent, Journal of Physical Oceanography, 4, 104-108, 1974.

FIGURE CAPTIONS

Figure 1. Examples of temperature gradient spectra compared to the 1-D Batchelor spectrum (dashed) and the noise. Broad spectral peaks from regions B and C may result from large variations of ϵ in microstructure regions. Patch numbers correspond to Table 1.

Figure 2. Temperature as a function of horizontal distance for records A, B, C and D selected for analysis from the total record of 8.3 km. The locations and extents of the most active microstructure patches are shown, along with identification numbers used in the summary of computed statistical parameters for each patch in Table 1, and in Figures 1, 3, 4, 5 and 6. Measurements were made on September 7, 1977 (Julian Day 250) from a towed body in the depth interval 30-40 m within the seasonal thermocline.

Figure 3. Conductivity gradient spectra from microstructure patches A-1 and A-4 compared to the noise. For $k > 1$ cpcm the spectrum from A-4 shows a salinity viscous convective subrange above the noise. The salinity dissipation rate χ_S can be inferred from χ_T and the ratio ϕ_S/ϕ_T of salinity and temperature viscous convective subranges, as shown. The salinity dominated portion of the conductivity spectrum from patch A-1 is below the noise. For patch A-4 $\chi_S = 2.2 \times 10^{-7}$ $(‰)^2 s^{-1}$ and $C_S = 500{,}000$.

Figure 4. Comparison of ϵ values measured in the seasonal thermocline during MILE. Patch values from the towed body (numbered open squares from Table 1) are overlapped by patch values (open circles and triangles) from the Dillon and Caldwell (1980) dropsonde, giving good agreement. ϵ_o and ϵ_o' values from Table 1 are indicated by numbered points and crossed squares, showing that ϵ values for the patches before the time of observation were much larger. Note that the ϵ values for patches D-3, D-4 and D-5 are in the completely fossil range, as

shown above, and are about 10^5 less than their previous ϵ_o values at fossilization. The Lange (1981) heated thermistor ϵ profiles are surprisingly large considering that the corresponding χ profiles shown in Fig. 5 are so small. The upper plot shows the buoyancy and viscous scales corresponding to the ϵ values below, with $N = 2.4 \times 10^{-2}$ rad/sec. The range of wavelengths λ which can be actively turbulent is $1.2\, L_R \geqslant \lambda \geqslant 15\, L_K$ according to Gibson (1981b, 1982a), and is shown by the crosshatched region. All microstructure patches with $\epsilon < 10^{-4}$ cm^2/s^3 are completely fossil turbulence. Mean values $\bar{\epsilon}$, $\bar{\epsilon}'$ and $\bar{\epsilon}_o$ from Table 1 are shown.

Figure 5. Comparison of χ and C values measured in the seasonal thermocline during MILE. Patch values of χ from the towed body (numbered open squares, from Table 1) are overlapped by the patch values inferred from Dillon and Caldwell (1980) assuming $\partial \bar{T}/\partial z = 0.3$ °C m^{-1} (open circles and triangles), giving good agreement. Lange (1981) χ profiles also shown on the figure are somewhat larger than $\chi_{MODE} = 4 \times 10^{-10}$ °C^2/s from the lognormal probability distribution function for χ measured by Washburn and Gibson (1982b), but are much less than the patch χ values or χ_{MEAN}. χ_o and C_o values at fossilization from Table 1 are indicated by numbered crossed squares, and show that previous values were larger by factors of $10^1 - 10^2$, not so large as the factors of 10^5 for ϵ shown in Fig. 4.

Figure 6. Turbulence activity parameter A_T versus C for data of Table 1. Record A patches are numbered open circles, Record B triangles and Record D squares. The solid line is from Caldwell et al. (1980) and Gibson (1982c), and shows that the Caldwell et al. (1980) MILE dropsonde data is either completely fossil ($\gamma < 5N$) or fossil at large scales (the triangular "fossil+active" region where $1 \geqslant A_T \geqslant 4.4/C^{1/2}$). Extrapolation of C values to a point $\leqslant C_o$ is illustrated by the dashed line for patch D-4 using (7). Note that according to Caldwell et al. (1980) A_T should have a constant value 0.18 rather than the wide scatter over a range of 2 decades observed.

Figure 7. Comparison of $\epsilon'_o = 13DCN^2$ with a similar quantity inferred from the bandpassed temperature variance $\epsilon''_o = [2\,\delta T_{rms}\,(\partial\bar{T}/\partial z)^{-1}]^2 N^3$. The wavenumber passband for δT_{rms} is $0.02 \leqslant k \leqslant 1$ cpcm.

Figure 8. Comparison of horizontal profiles of bandpassed temperature variance $\overline{(\delta T)^2}$ with temperature gradient variance for a 400 m section of data containing microstructure patch D-4 (at 275 m). The passband for both $\overline{(\delta T)^2}$ and $\overline{(\partial T/\partial x)^2}$ is $0.02 \leqslant k \leqslant 1$cpm. The similarity between the two profiles shows that bandpassed variance $(\delta T)^2$ is a good indicator of diffusive scale temperature gradient activity.

Figure 9. Temperature and temperature gradient spectra for for patch D-4 from the record of Fig. 8 in variance preserving form. Note the separation in wavenumber between the portions of the spectra which dominate $(\delta T)^2$ and $(\partial T/\partial x)^2$ shown in Fig. 8 and ϵ''_o and ϵ'_o shown in Fig. 7.

Figure 10. Comparison of $A_T^2 = \epsilon/\epsilon'_o$ with ϵ/ϵ''_o for 33 patches from Table 1. Small values of ϵ/ϵ'_o and ϵ/ϵ''_o indicate that the dissipation rates ϵ in the patches were higher before observation. ϵ'_o is an estimator of the dissipation rate required to produce the observed Cox number while ϵ''_o is an estimator of the rate required to overturn on an inferred vertical scale L_T'' defined in Fig. 7.

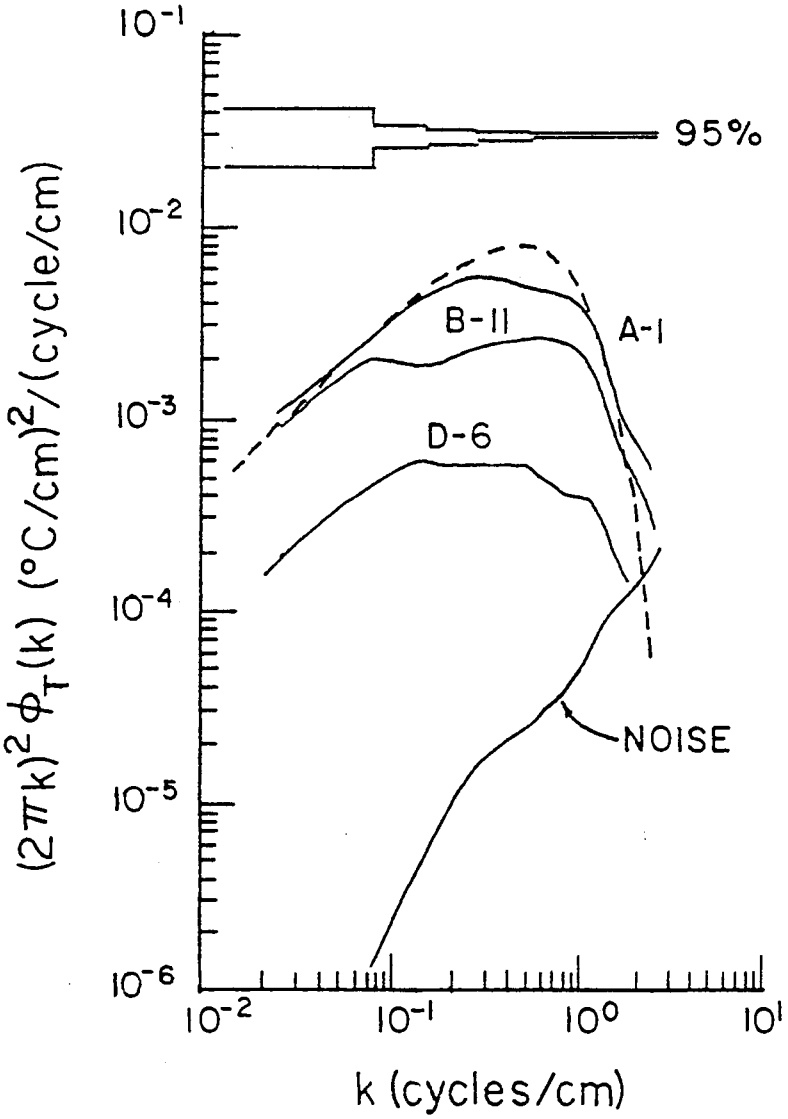

SPECTRUM	COX NO.
A-I	2650
B-II	1393
D-6	277
- - - - -	1-D BATCHELOR (1959) SPECTRUM

Fig. 1

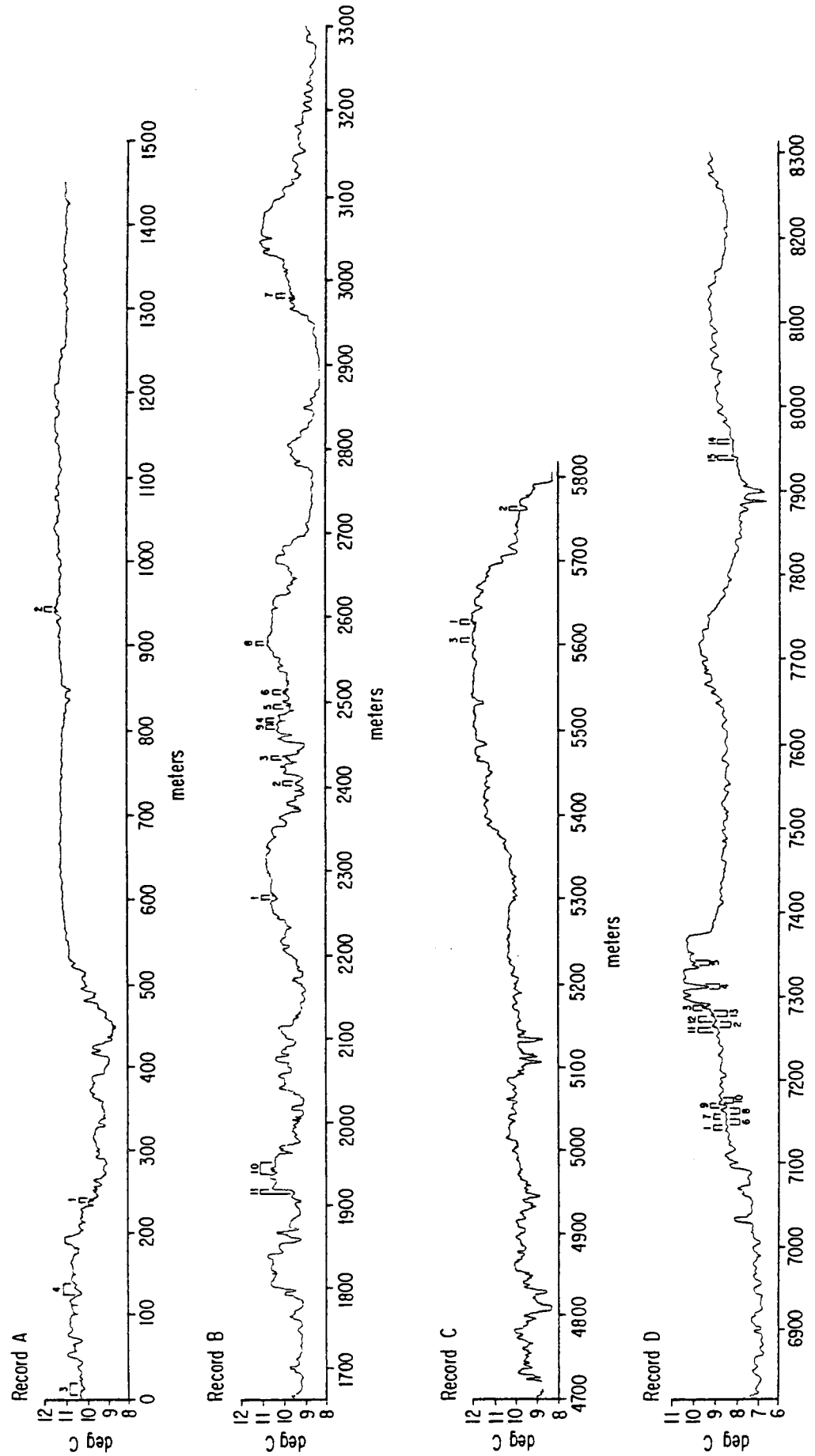
Record A
deg C
meters
Record B
deg C
meters
Record C
deg C
meters
Record D
deg C
meters

Fig. 2

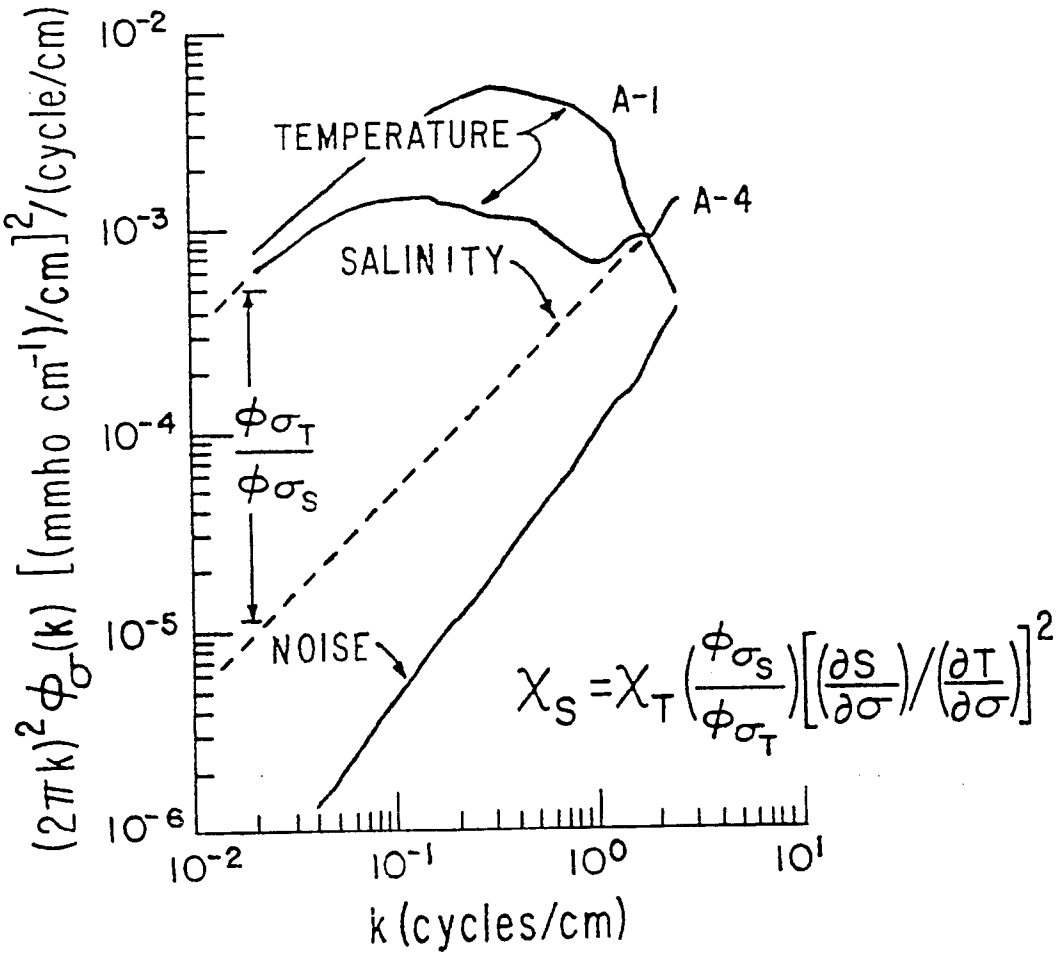
$(2\pi k)^2 \phi_\sigma(k)$ [(mmho cm^{-1})/cm]^2/(cycle/cm)
10^{-2}
10^{-3}
10^{-4}
10^{-5}
10^{-6}
TEMPERATURE
A-1
A-4
SALINITY
$\phi\sigma_T$
$\phi\sigma_S$
NOISE
$\chi_S = \chi_T \left(\frac{\phi\sigma_S}{\phi\sigma_T}\right)\left[\left(\frac{\partial S}{\partial\sigma}\right)/\left(\frac{\partial T}{\partial\sigma}\right)\right]^2$
10^{-2}
10^{-1}
10^{0}
10^{1}
k (cycles/cm)

Fig. 3

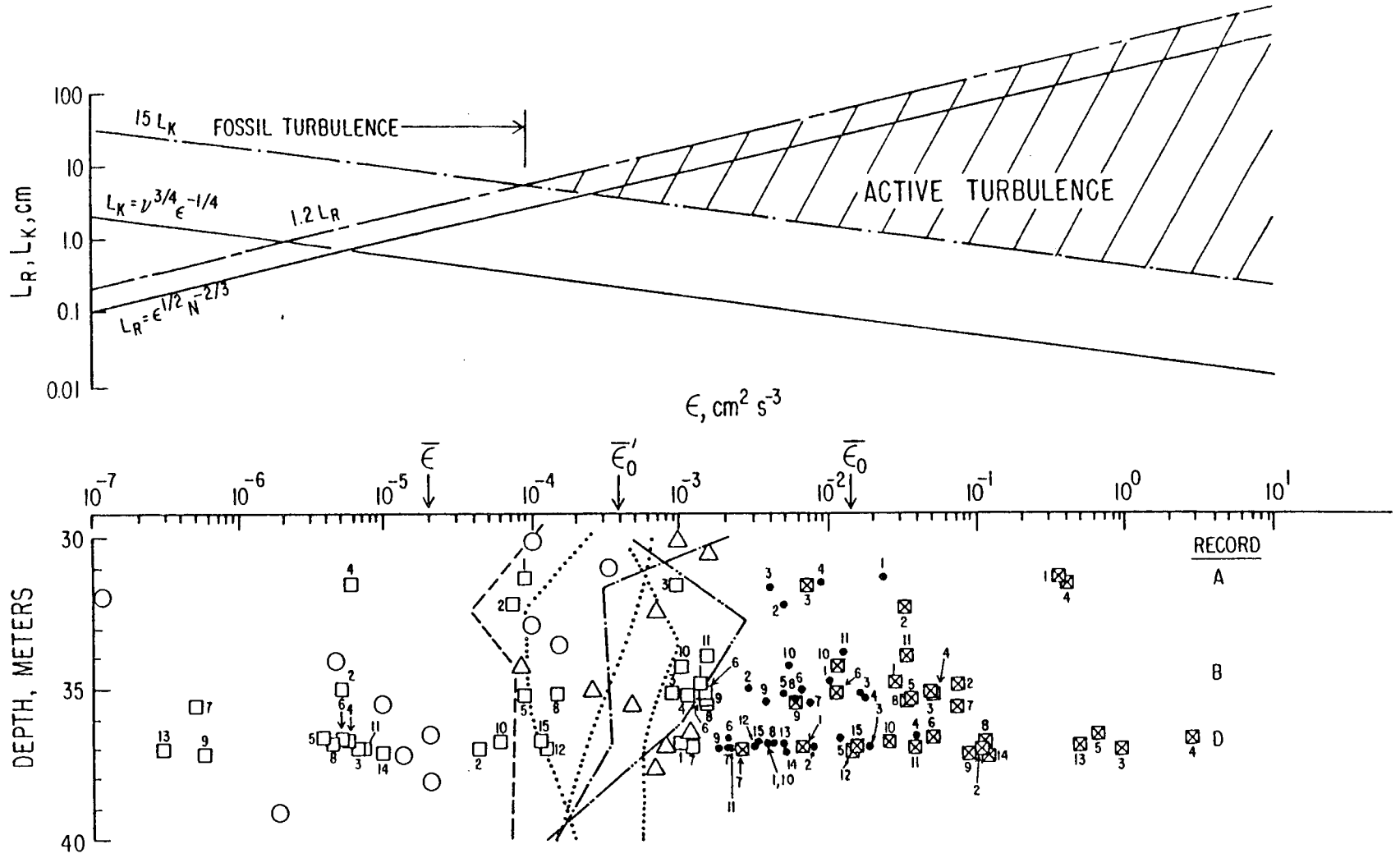

LANGE (1981) DROPSONDE
ϵ PROFILES

	DROP	WIND	JD
– – – –	24	8 m/s	245
— · —	25	6 m/s	246
— · · —	26	6 m/s	246
.....	WING		

DILLON AND CALDWELL (1980)
DROPSONDE ϵ PATCHES

	WIND	JD
○	5.5 m/s	244,0542
△	15.5 m/s	244,1111

UCSD TOWED BODY
(DATA FROM TABLE I)
$\epsilon, \epsilon_0', \epsilon_0$ PATCHES

		WIND	JD
ϵ	□	7.7 m/s	250
ϵ_0'	•	$\epsilon_0' = 13\ DCN^2$	
ϵ_0	⊠	$\epsilon_0 = 13\ DC_0N^2$	

Fig. 4

Journal of Cosmology (2013), Vol. 21, No. 32, pp 9934-9988.

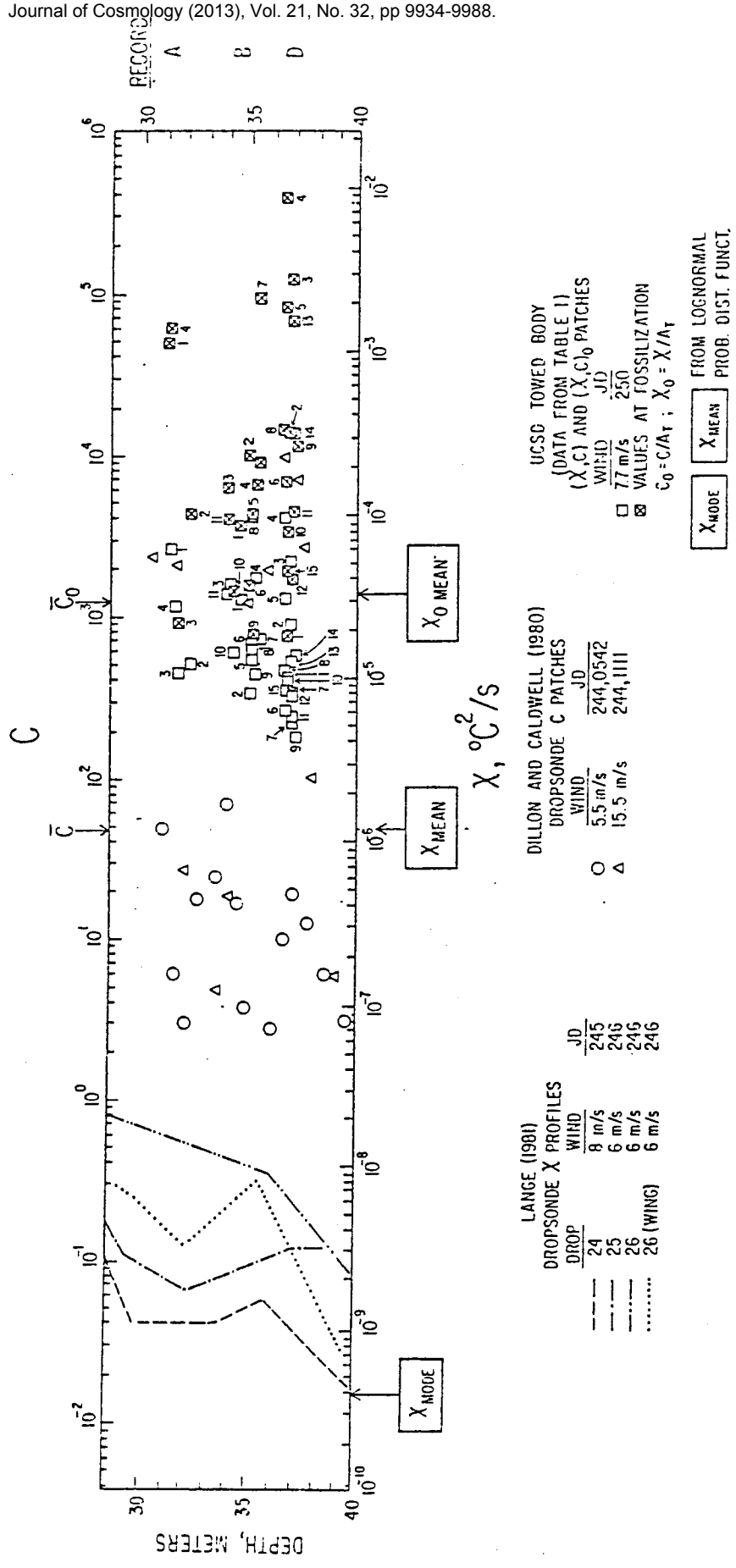
RECORD
A
B
D
C
$\bar{C}_0$
$\bar{C}$
χ_{MEAN}
$\chi_{O\ MEAN}$
χ_{MODE}
χ, °C²/S
DEPTH, METERS
LANGE (1981)
DROPSONDE χ PROFILES
DROP WIND JD
24 8 m/s 245
25 6 m/s 246
26 6 m/s 246
26 (WING) 6 m/s 246
DILLON AND CALDWELL (1980)
DROPSONDE C PATCHES
WIND JD
○ 5.5 m/s 244.0542
△ 15.5 m/s 244.1111
UCSD TOWED BODY
(DATA FROM TABLE 1)
(χ,C) AND (χ,C)₀ PATCHES
WIND JD
□ 7.7 m/s 250
⊠ VALUES AT FOSSILIZATION
$C_0 = C/A_T$; $\chi_0 = \chi/A_T$
χ_{MODE} χ_{MEAN} FROM LOGNORMAL
PROB. DIST. FUNCT.

Fig. 5

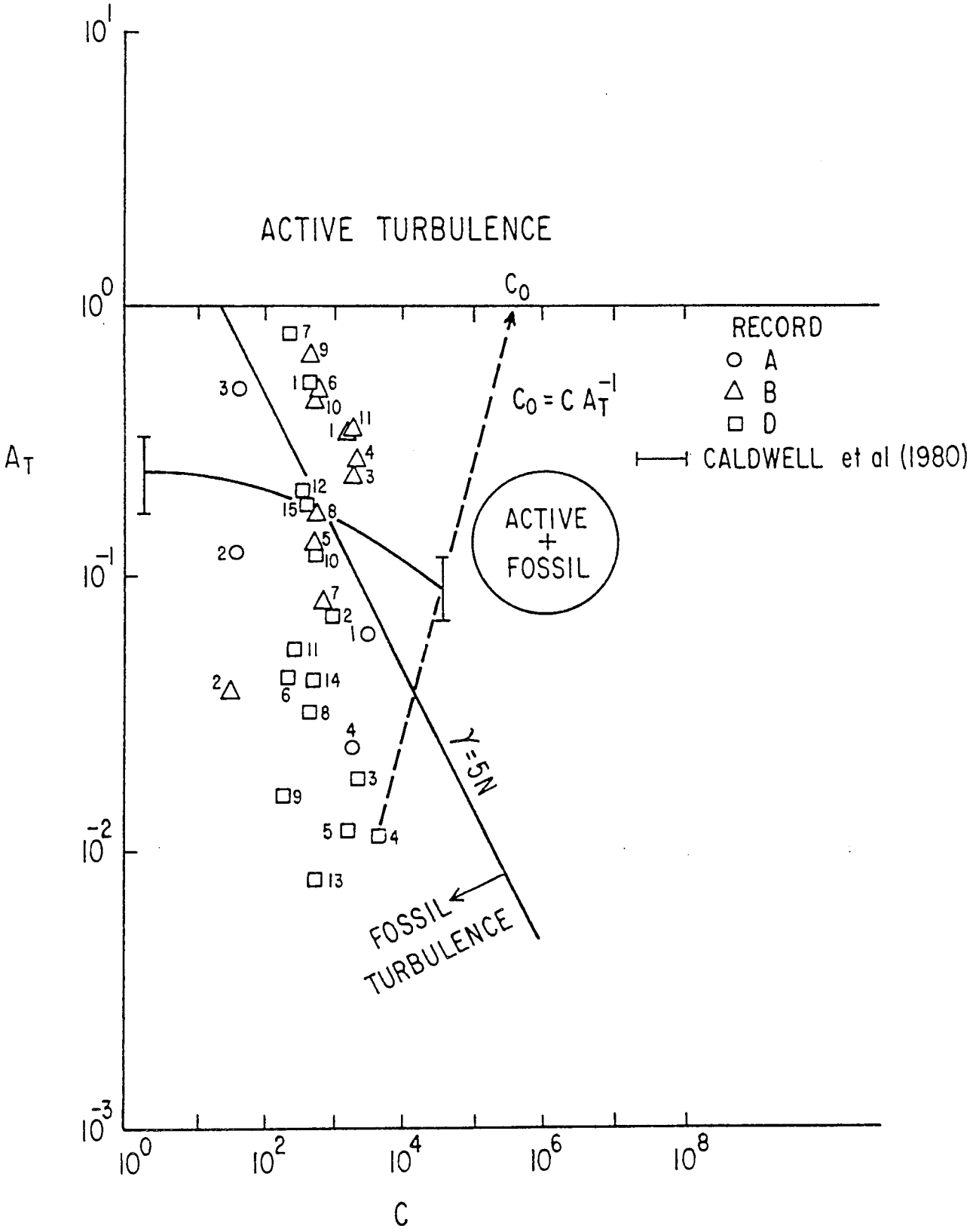
ACTIVE TURBULENCE
C_0
$C_0 = C A_T^{-1}$
RECORD
A
B
D
CALDWELL et al (1980)
ACTIVE + FOSSIL
$\gamma = 5N$
FOSSIL TURBULENCE
A_T
C
10^1
10^0
10^{-1}
10^{-2}
10^{-3}
10^0
10^2
10^4
10^6
10^8

Fig. 6

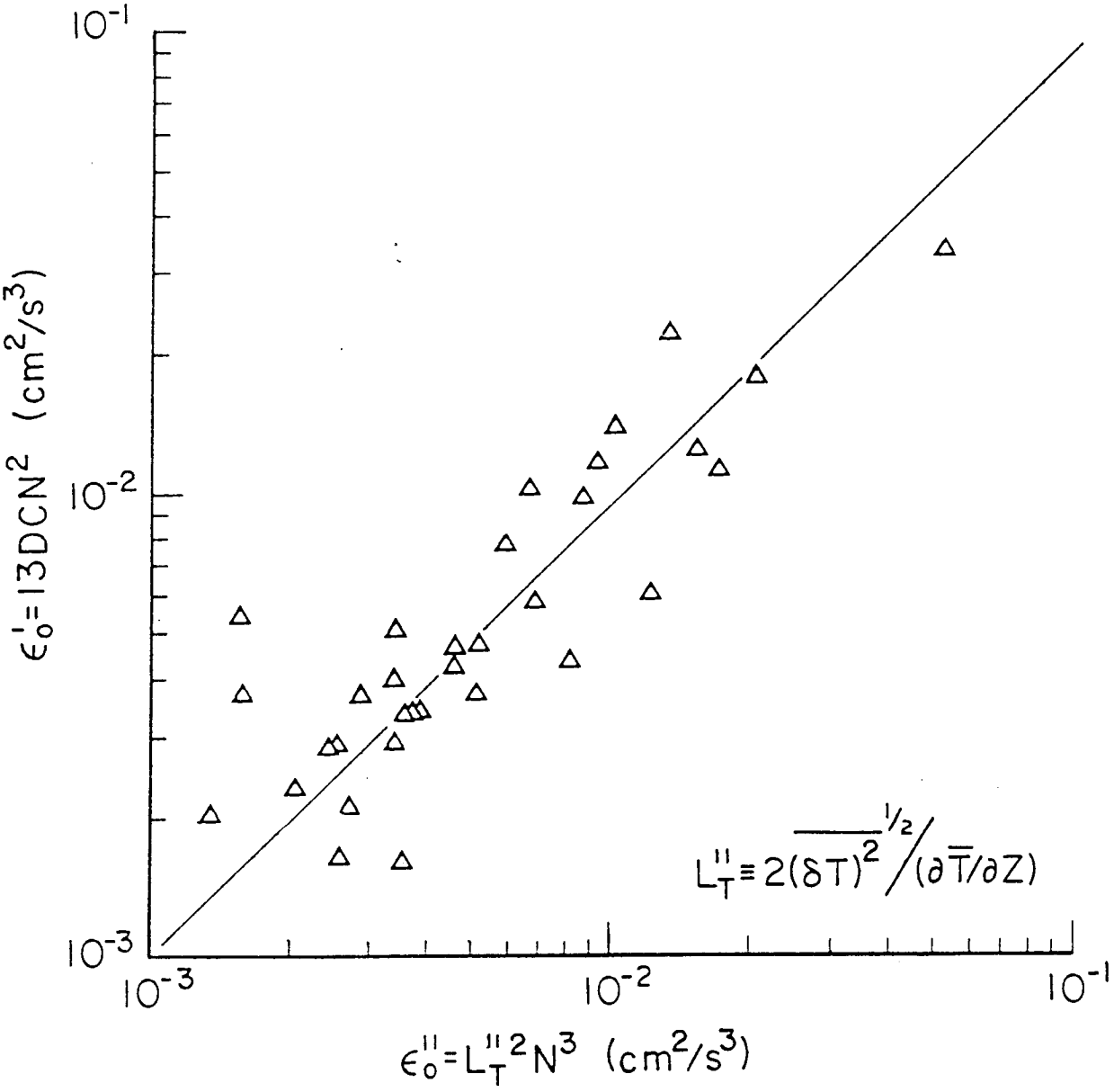
10^{-1}
10^{-2}
10^{-3}
$\epsilon_o' = 13DCN^2$ (cm^2/s^3)
10^{-3}
10^{-2}
10^{-1}
$L_T'' \equiv 2\overline{(\delta T)^2}^{1/2} / (\partial \bar{T}/\partial Z)$
$\epsilon_o'' = L_T''^2 N^3$ (cm^2/s^3)

Fig. 7

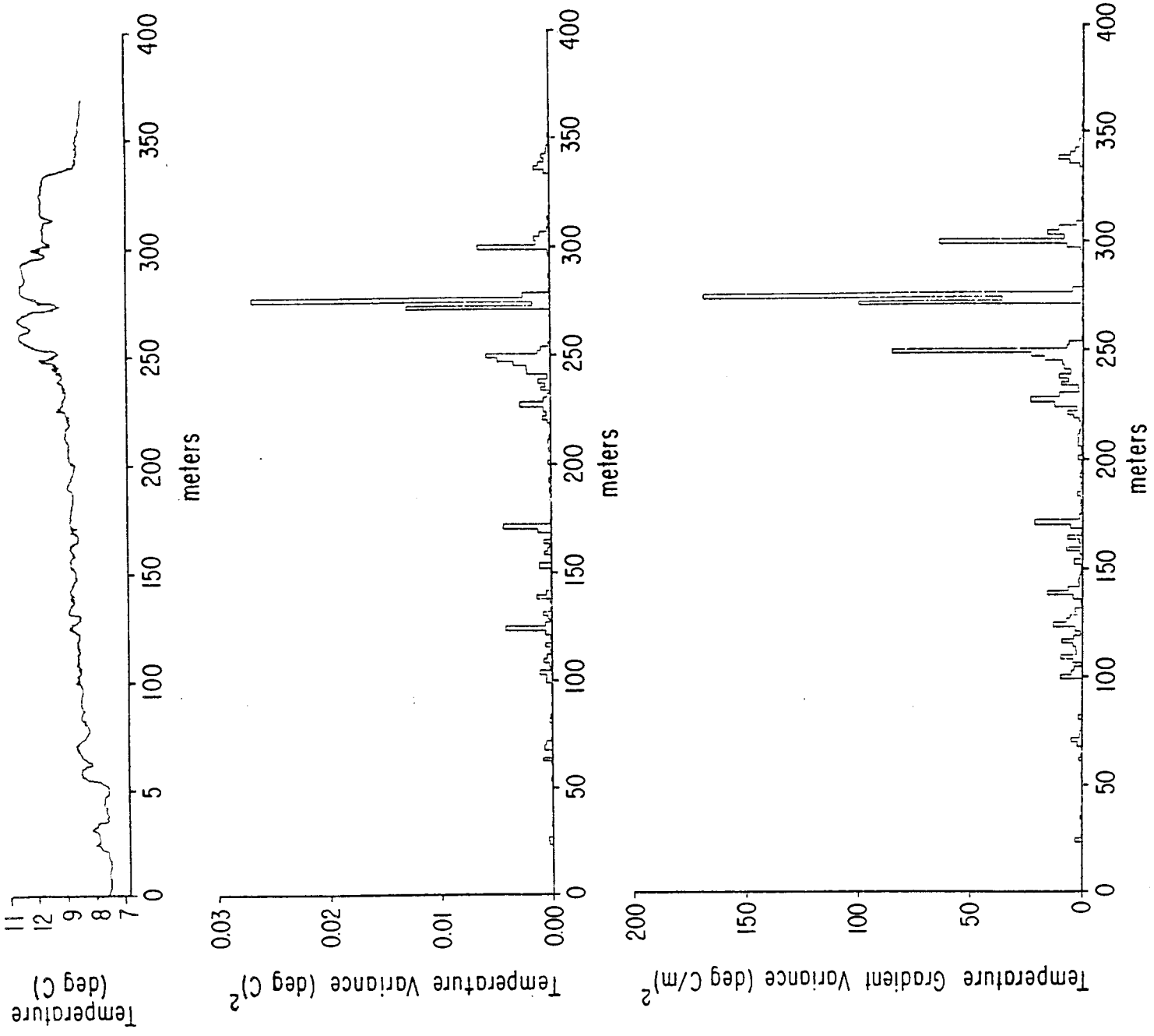
Temperature (deg C)
11
12
9
8
7
0
5
100
150
200
250
300
350
400
meters
Temperature Variance (deg C)^2
0.03
0.02
0.01
0.00
0
50
100
150
200
250
300
350
400
meters
Temperature Gradient Variance (deg C/m)^2
200
150
100
50
0
0
50
100
150
200
250
300
350
400
meters

Fig. 8

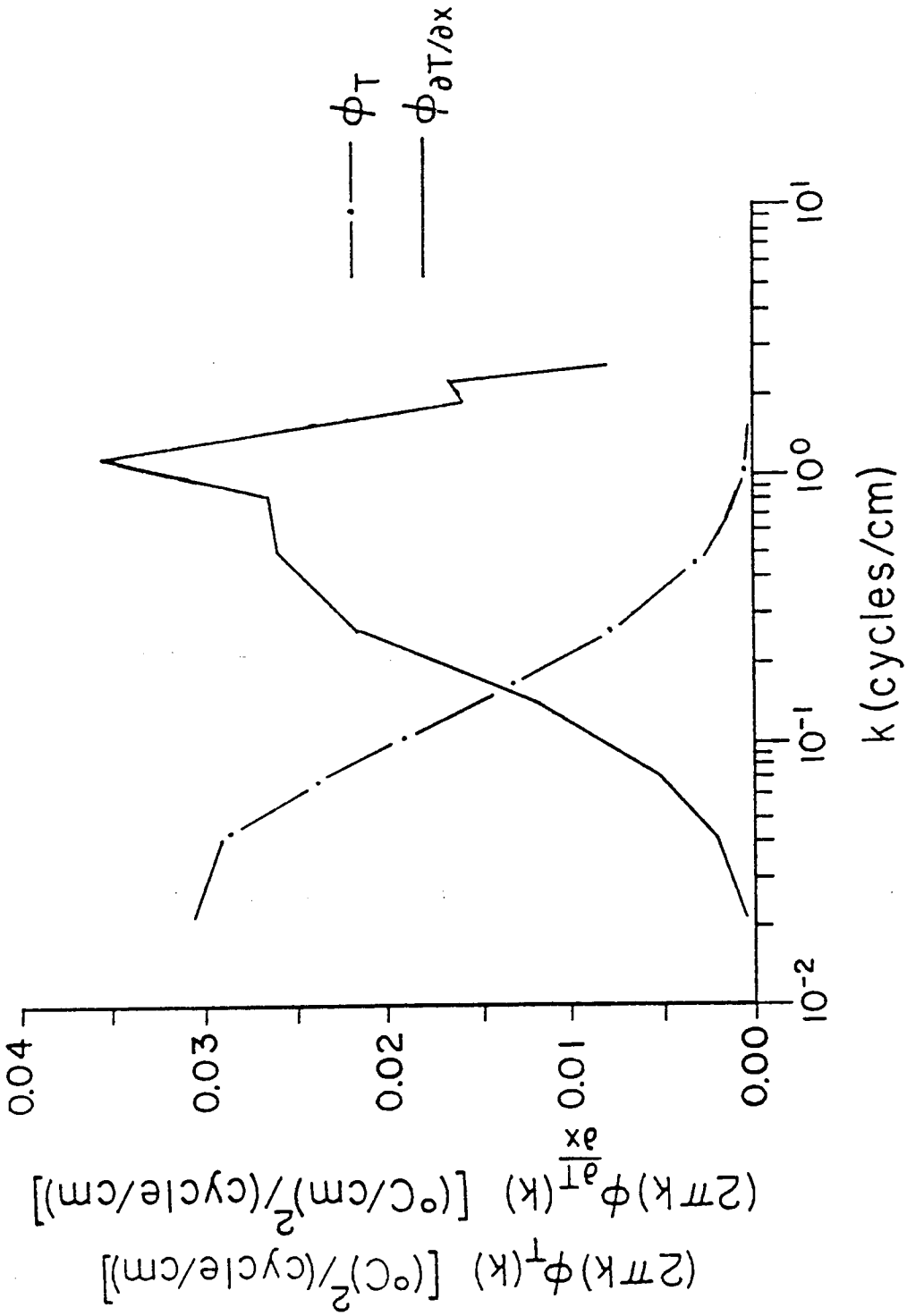
$(2\pi k)\phi_T(k)$ [(°C)²/(cycle/cm)]
$(2\pi k)\phi_{\frac{\partial T}{\partial x}}(k)$ [(°C/cm)²/(cycle/cm)]
0.04
0.03
0.02
0.01
0.00
10^{-2}
10^{-1}
10^{0}
10^{1}
k (cycles/cm)
ϕ_T
$\phi_{\partial T/\partial x}$

Fig. 9

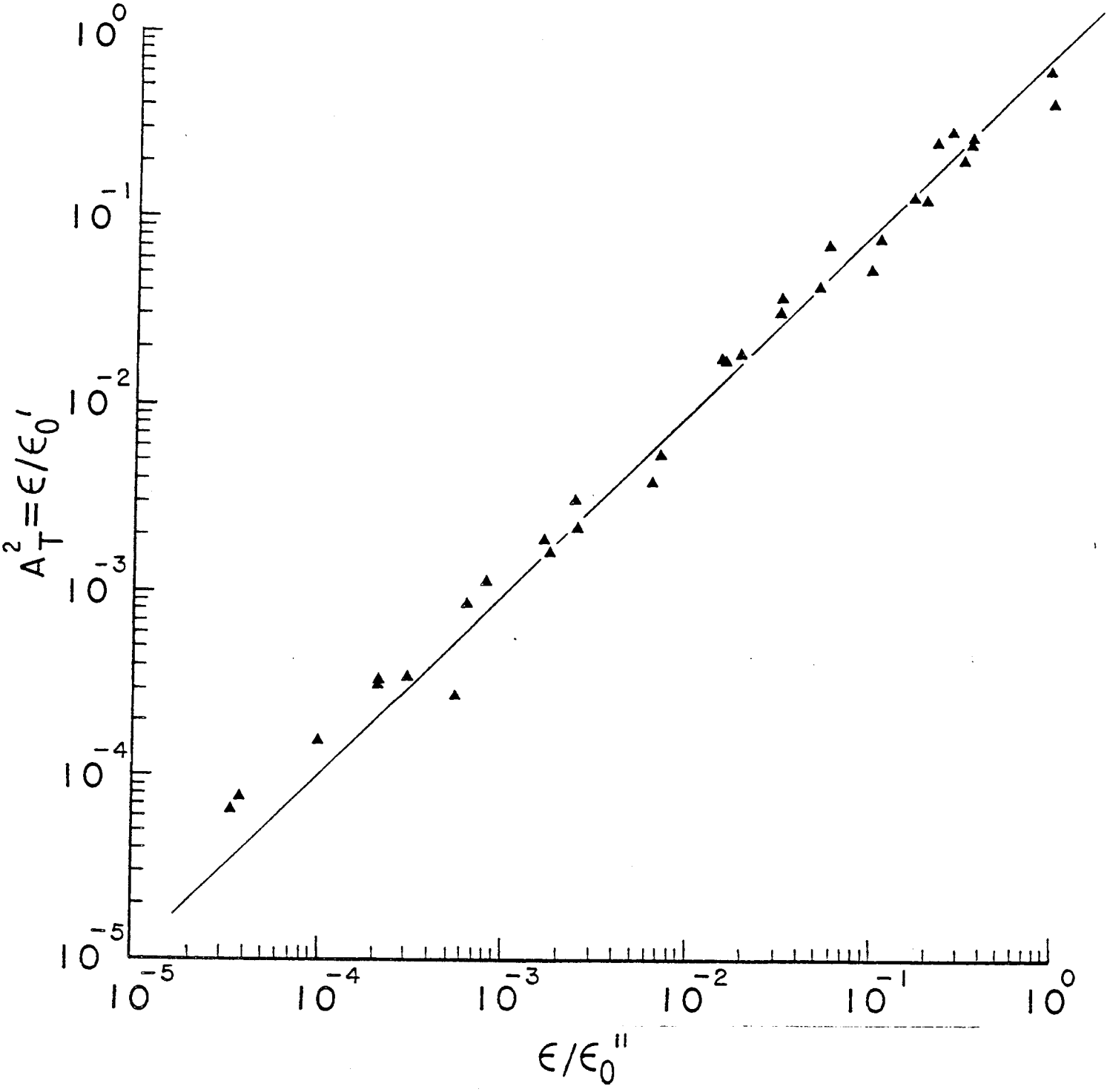
10^{0}
10^{-1}
10^{-2}
10^{-3}
10^{-4}
10^{-5}
$A_T^2 = \epsilon/\epsilon_0'$
10^{-5}
10^{-4}
10^{-3}
10^{-2}
10^{-1}
10^{0}
ϵ/ϵ_0''

Fig. 10

TABLE I. Turbulence and mixing parameters of the dominant microstructure patches.

Record	Patch	Depth m	Rec. length m	C	γ/N	A_T	ϵ cm^2/s^3	χ_T °C^2/s	χ_S ‰^{2}/s	ϵ'_o cm^2/s^3	ϵ''_o cm^2/s^3	ϵ_o cm^2/s^3	χ_{T_o} °C^2/s
A	1	31.3	6.6	2650	3.9	6.2×10^{-2}	8.4×10^{-5}	6.7×10^{-5}		2.2×10^{-2}	1.4×10^{-2}	3.6×10^{-1}	1.1×10^{-3}
	2	32.2	6.6	501	3.6	1.3×10^{-1}	7.1×10^{-5}	1.3×10^{-5}	5.8×10^{-8}	4.2×10^{-3}	4.6×10^{-3}	3.2×10^{-2}	9.7×10^{-5}
	3	31.6	15.0	436	13.2	5.2×10^{-1}	9.7×10^{-4}	1.1×10^{-5}	2.9×10^{-7}	3.7×10^{-3}	2.9×10^{-3}	7.1×10^{-3}	2.1×10^{-5}
	4	31.5	12.6	670	1.0	3.1×10^{-2}	5.5×10^{-6}	1.7×10^{-5}	2.2×10^{-7}	5.7×10^{-3}	8.8×10^{-3}	4.2×10^{-1}	1.3×10^{-3}
B	1	34.7	6.6	1220	15.1	3.5×10^{-1}	1.3×10^{-3}	3.1×10^{-5}		1.0×10^{-2}	6.7×10^{-3}	2.9×10^{-2}	8.7×10^{-5}
	2	35.0	5.7	343	0.9	4.0×10^{-2}	4.6×10^{-6}	8.6×10^{-6}	1.5×10^{-7}	2.9×10^{-3}	2.6×10^{-3}	7.2×10^{-2}	2.2×10^{-4}
	3	35.1	4.8	1494	12.5	2.6×10^{-1}	8.7×10^{-4}	3.8×10^{-5}	1.3×10^{-7}	1.3×10^{-2}	1.5×10^{-2}	4.8×10^{-2}	1.4×10^{-4}
	4	35.3	4.6	1688	14.0	2.8×10^{-1}	1.1×10^{-3}	4.3×10^{-5}	1.0×10^{-7}	1.4×10^{-2}	1.0×10^{-2}	5.1×10^{-2}	1.5×10^{-4}
	5	35.1	4.4	553	3.9	1.4×10^{-1}	8.6×10^{-5}	1.4×10^{-5}		4.7×10^{-3}	4.6×10^{-3}	3.4×10^{-2}	1.0×10^{-4}
	6	35.1	4.2	695	16.3	5.0×10^{-1}	1.5×10^{-3}	1.8×10^{-5}		5.8×10^{-3}	6.9×10^{-3}	1.2×10^{-2}	3.5×10^{-5}
	7	35.6	4.6	716	0.3	8.6×10^{-3}	4.5×10^{-7}	1.8×10^{-5}		6.0×10^{-3}	1.2×10^{-2}	7.0×10^{-1}	2.1×10^{-3}
	8	35.1	3.8	323	5.2	2.4×10^{-1}	1.5×10^{-4}	8.1×10^{-6}	2.9×10^{-7}	2.7×10^{-3}		3.2×10^{-2}	4.9×10^{-5}
	9	35.3	5.9	440	16.5	6.4×10^{-1}	1.5×10^{-3}	1.1×10^{-5}		3.7×10^{-3}	1.6×10^{-3}	5.8×10^{-3}	1.7×10^{-5}
	10	34.2	14.8	601	13.6	4.5×10^{-1}	1.0×10^{-3}	1.5×10^{-5}		5.1×10^{-3}	3.4×10^{-3}	1.1×10^{-2}	3.4×10^{-5}
	11	34.0	5.0	1393	16.5	3.6×10^{-1}	1.5×10^{-3}	3.5×10^{-5}		1.2×10^{-2}	9.4×10^{-3}	3.3×10^{-2}	9.8×10^{-5}
C	1	35.9	6.8	477	14.1	5.3×10^{-1}	1.1×10^{-3}	1.2×10^{-5}		4.0×10^{-3}	3.3×10^{-3}	7.6×10^{-3}	2.3×10^{-5}
	2	35.8	6.3	390	4.3	1.8×10^{-1}	1.0×10^{-4}	9.8×10^{-6}		3.3×10^{-3}	3.6×10^{-3}	1.9×10^{-2}	5.6×10^{-5}
	3	37.3	5.8	396	0.4	1.6×10^{-2}	8.8×10^{-7}	1.0×10^{-5}		3.3×10^{-3}	1.6×10^{-3}	2.0×10^{-1}	6.1×10^{-4}
D	1	36.9	7.0	404	13.2	5.4×10^{-1}	9.7×10^{-4}	1.0×10^{-5}		3.4×10^{-3}	3.7×10^{-3}	6.3×10^{-3}	1.9×10^{-5}
	2	37.0	7.9	920	2.7	7.3×10^{-2}	4.1×10^{-5}	2.3×10^{-5}		7.7×10^{-3}	6.0×10^{-3}	1.1×10^{-1}	3.2×10^{-4}
	3	37.0	6.6	2120	1.1	1.9×10^{-2}	6.2×10^{-6}	5.3×10^{-5}		1.8×10^{-2}	2.1×10^{-2}	9.6×10^{-1}	2.9×10^{-3}
	4	36.8	6.9	4009	1.0	1.2×10^{-2}	5.1×10^{-6}	1.0×10^{-4}		3.4×10^{-2}	5.3×10^{-2}	2.7×10^{0}	8.2×10^{-3}
	5	36.8	7.6	1360	0.8	1.8×10^{-2}	3.6×10^{-6}	3.4×10^{-5}		1.1×10^{-2}	1.7×10^{-2}	6.5×10^{-1}	1.9×10^{-3}
	6	36.8	7.0	277	1.0	4.6×10^{-2}	5.0×10^{-6}	7.0×10^{-6}		2.3×10^{-3}	2.1×10^{-3}	5.0×10^{-2}	1.5×10^{-4}
	7	37.0	6.6	241	14.8	7.8×10^{-1}	1.2×10^{-3}	6.1×10^{-6}		2.0×10^{-3}	1.3×10^{-3}	2.6×10^{-3}	7.8×10^{-6}
	8	36.9	7.3	442	0.9	3.3×10^{-2}	4.1×10^{-6}	1.1×10^{-5}		3.7×10^{-3}	5.2×10^{-3}	1.1×10^{-1}	3.3×10^{-4}
	9	37.1	6.5	193	0.3	1.8×10^{-2}	5.3×10^{-7}	4.9×10^{-6}		1.6×10^{-3}	2.6×10^{-3}	8.9×10^{-2}	2.7×10^{-4}
	10	36.9	7.2	403	3.2	1.3×10^{-1}	5.8×10^{-5}	1.0×10^{-5}		3.4×10^{-3}	3.9×10^{-3}	2.6×10^{-2}	7.7×10^{-5}
	11	37.0	6.5	250	1.1	5.5×10^{-2}	6.4×10^{-6}	6.3×10^{-6}		2.1×10^{-3}	2.7×10^{-3}	3.8×10^{-2}	1.1×10^{-4}
	12	37.0	6.0	334	4.7	2.1×10^{-2}	1.2×10^{-4}	8.4×10^{-6}		2.8×10^{-3}	2.4×10^{-3}	1.4×10^{-2}	4.1×10^{-5}
	13	37.0	7.7	518	0.2	8.0×10^{-3}	2.8×10^{-7}	1.3×10^{-5}		4.4×10^{-3}	8.3×10^{-3}	5.4×10^{-1}	1.6×10^{-3}
	14	37.1	6.1	560	1.3	4.3×10^{-2}	8.6×10^{-6}	1.4×10^{-5}		4.7×10^{-3}	5.2×10^{-3}	1.1×10^{-1}	3.3×10^{-4}
	15	36.9	6.2	346	4.4	1.9×10^{-1}	1.1×10^{-4}	8.7×10^{-6}		2.9×10^{-3}	3.4×10^{-3}	1.5×10^{-2}	4.5×10^{-5}

$N = 12.3$ cph, 2.2×10^{-2} rad/s

$\partial\bar{T}/\partial z = 0.3$ °C/m

$\epsilon'_o = 13DC\,N^2$

$\epsilon''_o = L''^2_T\,N^3,\ L''_T = 2\overline{\delta T^2}^{1/2}/\partial\bar{T}/\partial z$

$\epsilon_o = \epsilon_o/A_T$

$$\chi_S = \chi_T\left(\phi\sigma_S/\phi\sigma_T\right)\left|\left(\frac{\partial S}{\partial\sigma}\right)/\left(\frac{\partial T}{\partial\sigma}\right)\right|^2$$

Journal of Cosmology (2013), Vol. 21, No. 32, pp 9934-9988.

Note that the extreme intermittency of turbulence in natural flows like the ocean, clearly shown in this pioneering study of Washburn and Gibson, is the key physical process responsible for catastrophic equatorial icing events that have killed hundreds of airplane passengers and crew and consumed billions of dollars searching the ocean bottom in questionable locations suggested by conspiracy theories. CHG (see JofC Vol. 21, 22, etc.). Skepticism and pressures of the oceanographic community about the existence of fossil turbulence and turbulence intermittency led Prof. Washburn (then a postdoc) to wisely request delay of publication of this paper. Neither of us anticipated that such a state of ignorance, which still persists, could kill anyone or waste so much time and money.